phil 280
12/27/66

IDO-17202

NUCLEAR TECHNOLOGY BRANCHES QUARTERLY REPORT

April 1 - June 30, 1966

PHILLIPS PETROLEUM COMPANY

PHILLIPS 66

ATOMIC ENERGY DIVISION

NATIONAL REACTOR TESTING STATION
US ATOMIC ENERGY COMMISSION

3.00

PRINTED IN USA. PRICE ~~$2.00~~ AVAILABLE FROM THE CLEARINGHOUSE FOR FEDERAL SCIENTIFIC AND TECHNICAL INFORMATION, NATIONAL BUREAU OF STANDARDS, U. S. DEPARTMENT OF COMMERCE, SPRINGFIELD, VIRGINIA 22151

IDO-17202
AEC Research and Development Report
Reactor Technology
TID-4500
Issued: November 1966

NUCLEAR TECHNOLOGY BRANCHES QUARTERLY REPORT

APRIL 1 - JUNE 30, 1966

D. R. deBoisblanc
ASSISTANT MANAGER
ATOMIC ENERGY DIVISION

W. C. Francis
MANAGER,
REACTOR ENGINEERING

R. G. Fluharty
MANAGER,
NUCLEAR TECHNOLOGY

PHILLIPS
PETROLEUM
COMPANY

Atomic Energy Division
Contract AT(10-1)-205
Idaho Operations Office
U. S. ATOMIC ENERGY COMMISSION

Previous Quarterly Reports in the MTR-ETR Series

Quarter	Number	Quarter	Number
1959		1960	
1	IDO-16543	1	IDO-16633
2	IDO-16561	2	IDO-16648
3	IDO-16580	3	IDO-16658
4	IDO-16620	4	IDO-16665
1961		1962	
1	IDO-16695	1	IDO-16781
2	IDO-16710	2	IDO-16805
3	IDO-16733	3	IDO-16827
4	IDO-16760	4	IDO-16857
1963		1964	
1	IDO-16898	1	IDO-16994
2	IDO-16917	2	IDO-17042
3	IDO-16932	3	IDO-17052
4	IDO-16977	4	IDO-17081
1965		1966	
1	IDO-17104	1	IDO-17192
2	IDO-17140		
3	IDO-17147		
4	IDO-17191		

SUMMARY

The power distribution in the ATRC has been remeasured with better accuracy in determining the hot-spot fission rate. The radial profile of the void coefficient of reactivity in the ATRC fuel annulus was found to be more negative than anticipated. The excess reactivity of the ATRC 39-kg core was measured by uniformly poisoning the reactor.

Pulsed-neutron apparatus and experimental procedures used in the "Critical Facilites" section are summarized. The worths of the ATRC safety rods were measured in several different shim configurations using both the pulsed-neutron and rod-drop methods. With the latter method, the effect of the location of the neutron detector was investigated.

The worth of the ETRC safety rods was measured using the pulsed-neutron method. It was demonstrated in these measurements that the rod-worth values were generally independent of neutron-generator - neutron-detector geometry.

Results of inspections of ATR fuel elements fabricated under the first production contract are reported. The majority of the fuel elements appear satisfactory for ATR use.

Engineering calculations upon radially zone-loaded ATR fuel elements have shown lower plate temperatures and axial buckling stresses in comparison to the uniformly loaded, Mark-IV reference fuel.

Thermal compatibility studies were conducted on dispersions of UAl_3 particles in 300 Series stainless steel, Cr, Ni, and Nb. Samples were prepared by powder metallurgical techniques, heat-treated, and examined. Metallographic, X-ray diffraction, and electron-beam microprobe examinations were used to determine compatibility. At 800°C, the UAl_3 reacted only slightly with stainless steel and appeared compatible with the remaining materials. At 1200 to 1250°C, the UAl_3 underwent extensive reaction and diffusion with all of the matrix materials tested.

Compatibility tests between liquid lead, tin, and bismuth and uranium-aluminide fuels have shown that liquid lead should be a satisfactory heat transfer medium up to 600°C for short term use.

CONTENTS

FIGURES

TABLES

I. REACTOR ENGINEERING

1. CRITICAL FACILITIES
(E. E. Burdick)

1.1 Remeasurement of the 50-50-50 Power Distribution in the ATRC (J. L. Durney)

The nominally 50-50-50 power distribution mapping reported in the last quarterly report [1] has been repeated since significant improvements in positioning the flux monitors have been accomplished. It was found that the fission-rate peaking is not as severe as the earlier measurements had indicated although the power distribution obtained in this repeat measurement is essentially the same as that obtained in the earlier measurement. Detailed measurements were made in water channel No. 19 in several fuel elements in order to determine the extent of fission-rate peaking in expected hot-spot regions. The values obtained are shown in Figure I-1 together with the overall power distribution. The improved accuracy of the measurement has resulted in a hot-spot fission-rate value of 21.1 kW/g U-235 or a peak-to-core average of 3.29 which is about 19 percent less than the 4.08 value reported earlier. The estimated standard deviation for the peak-to-core average ratios, shown in Figure I-1, is 4 percent.

1.2 ATRC Fuel Annulus Void Coefficients of Reactivity (N. C. Kaufman)

The reactivity effects due to localized void formation in the current, 975-g U-235 ATRC fuel elements have been measured using Teflon to simulate the voids [a]. These measurements were made at the azimuthal center of coolant channels Nos. 1, 2, 10, 16, and 20 in fuel elements in Positions 12, 19, 32, and 39. The shape of the radial profile (shown in Figure I-2) was that which was expected although the values themselves were somewhat more negative than expected. Consequently, measurements in two of the same positions studied previously in 875-g fuel elements were repeated in the present 975-g elements. Figure I-3 shows a previously measured profile [3] obtained in a 50-50-50 power split with no experiments in the flux traps. The differences in these profiles may be, in part, due to side-plate vents [4] in the present elements and, to a much lesser extent, due to the absence of a fueled experiment in the adjacent flux trap in the present core.

It appears from these recent measurements that the negative fuel-element-void reactivity feedback will be greater in the 39-kg core than anticipated and that the positive effects in Channels 1 and 20 had been previously overestimated. It also appears that the onset of any nucleate boiling in Channel 19 will produce a negative reactivity effect and that any such boiling will be more easily detected than had been previously estimated.

1.3 ATR Safety Rod Worths from the Rod-Drop Method (N. C. Kaufman)

Measurements of the reactivity worth of the ATRC safety rods have been completed using the rod-drop method. In this method, the safety rods for

---

[a] The data here include a Teflon-to-air correction factor of 3.5 percent [2].

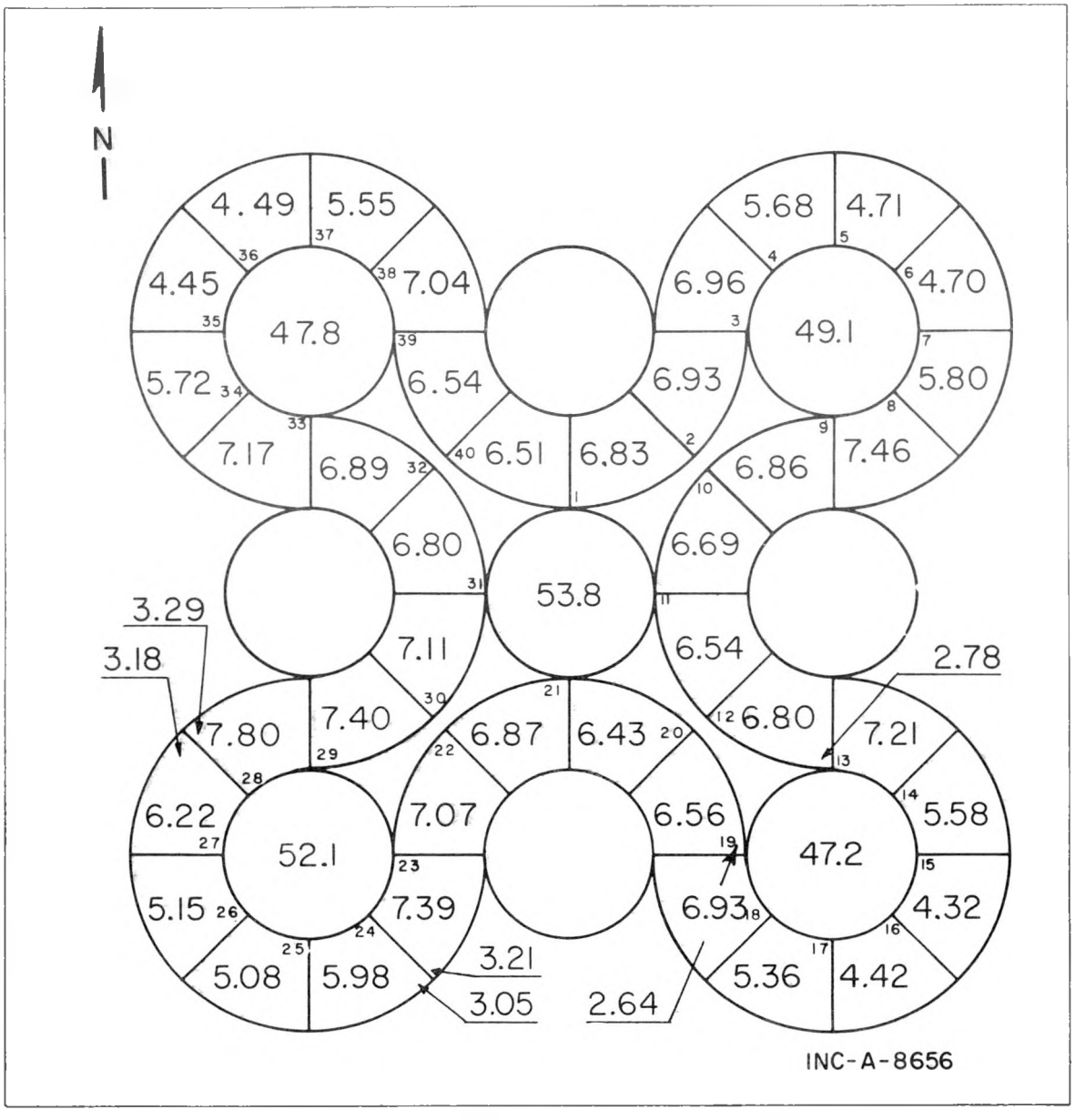

Fig. I-1 ATRC cross-section diagram showing the nominally 50-50-50 power distribution normalized to 250 MW. The numbers within the fuel elements are element powers in MW, and those in the inner flux traps are lobe powers (8 elements) in MW. Also, shown by arrows, are the ratios of the highest expected peak-to-core average fission rate ratios.

which a reactivity value is desired are rapidly inserted with the reactor just critical, and the resultant decrease of the neutron density, in time, is monitored with a detector and an associated fixed-interval counting system. The measurements reported here were done to determine the effect of shim configuration on the safety rod worth and to investigate the dependence of the results on the location of the neutron detector in the core. The safety rod worths have also been measured using the pulsed-neutron method as described in Section 1.5 below.

The ATRC safety rod worths were measured with two shim configurations: (a) outer shims withdrawn, neck shims inserted and (b) outer shims inserted, neck shims withdrawn. In both shim configurations, the safety rod reactivity

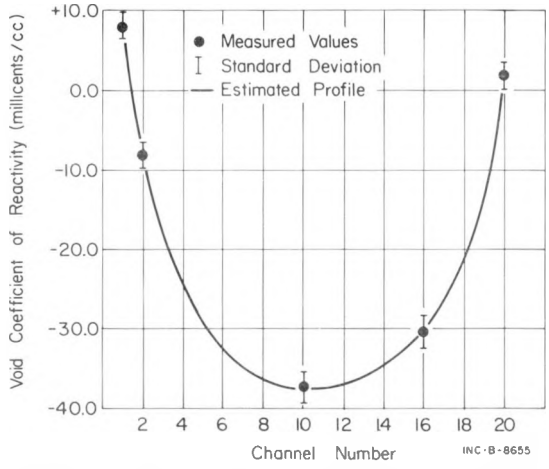

Fig. I-2 Void coefficient profile along the azimuthal center of ATRC fuel elements Nos. 12, 19, 32, and 39 in a nominally 50-50-50 power split with a 39-kg (U-235) core. Error bars represent one standard deviation estimated on the basis of five reproducibility measurements in the core containing no voids.

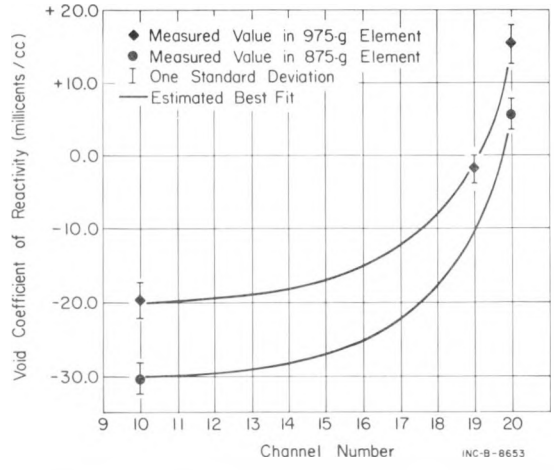

Fig. I-3 Void coefficient profile at hot-spot side of center in 875- and 975-g (U-235) ATRC fuel elements Nos. 12, 19, 32, 39 in a nominally 50-50-50 power split. Error bars represent one standard deviation estimated on the basis of five reproducibility measurements in the core containing no voids.

values, shown in Table I-1, indicate a rather marked dependence upon the position of the detector at which the measurements were made. This indicates

TABLE I-1

ATRC SAFETY ROD WORTHS OBTAINED WITH THE ROD-DROP METHOD

Run Number	Shim Configuration: Outers (deg)	Shim Configuration: Necks	Rods Dropped	Ion Chamber: Type	Ion Chamber: Position	Reactivity Worths[b] (dollars)
1	76	All inserted	NW, N, SW, S, SE(5)	Fission counter	Center flux trap above core	9.8 ± 0.2 9.7 ± 0.2[c]
2	76	All inserted	NW, N, SW, S, SE(5)	CIC-Log N No. 1 CIC-Log N No. 2	T5 midplane [a] T1 midplane [a]	13.1 ± 0.7 12.0 ± 0.5
3	76	All inserted	NW, N, SW, S, SE(5)	Fission counter	East flux trap above core	8.2 ± 0.2
4	0	Nos. 1 through 5 withdrawn	NW, N, SW, S, SE(5)	Fission counter	Center flux trap above core	8.3 ± 0.2 8.2 ± 0.2[c]
5	0	Nos. 1 through 5 withdrawn	NW, N, SW, S, SE(5)	CIC-Log N No. 1 CIC-Log N No. 2	T5 midplane [a] T1 midplane [a]	12.4 ± 0.7 11.0 ± 0.6
6	0	Nos. 1 through 5 withdrawn	NW, N, SW, S, SE(5)	Fission counter	Center flux trap below core	6.6 ± 0.1
7	0	Nos. 1 through 5 withdrawn	NW, N, SW, S, SE(5)	Fission counter	East flux trap above core	8.0 ± 0.1
8	76	All inserted	NW, SW, S, SE(4)	Fission counter	Center flux trap above core	6.6 ± 0.2

[a] Instrument thimbles outside reflector tank.

[b] Errors are estimates of one standard deviation based on the standard deviations of the ratios of recorded counts.

[c] Repeat run for reproducibility measurement.

that, in those core positions studied, the spatial neutron distribution following a safety rod insertion is quite different from that established at critical. For example, a comparison of the values for Runs 1 and 3 or Runs 4 and 7 in Table I-1 indicates that, relative to the critical distribution, the neutron density at a given point in time had decreased less in the east flux trap than in the center flux trap. A comparison of the values for Runs 4 and 6 indicates that at each point in time, the neutron density below the core had decreased less with respect to the critical distribution than had that above the core. This last effect would definitely be expected since the fully inserted safety rods remain 9 inches above the lower active fuel line thereby permitting the neutron density to be relatively greater at the bottom of the core than at the top.

The value obtained in Run 8 indicates that in the shim configuration used, the minimum worth of four ATRC safety rods is very near 5 percent $\Delta k/k$ for $\beta = 0.0075$. Previous measurements [5] have shown that a safety rod is worth more in an outer flux trap than in an inner flux trap. Thus, in Run 8, a minimum worth of four rods was obtained by preventing the rod in the N outer flux trap from inserting.

These data contain no interference from shim insertion since, in these rod drop experiments, the console key was turned off immediately following the safety rod insertion.

For all in-core measurements, a fission counter was used as a detector, and a resolution correction for this detector and its associated counting system was measured and applied to the data obtained with it. A ratio of the recorded counts following safety rod insertion to the recorded counts at critical was calculated for each of five 10-second count intervals. An average and a standard deviation for these ratios were obtained and interpreted in terms of reactivity using the equations developed by K. V. Moore [6] and tables supplied by S. R. Gossmann of the Instrumentation Analysis Section. These tables were similar to those provided by Moore but were obtained for the ATRC with present best estimates for ATRC safety rod calibration curves and kinetic parameters.

1.4 Critical Facilities Pulsed-Neutron Experimental Procedure and Apparatus (N. C. Kaufman)

The pulsed neutron technique for the measurement of reactivity and β/Λ has been used for about two years in the Critical Facilities Section. During those years, the experimental apparatus, procedure, and methods for data reduction have been evolving. The procedure and apparatus whose use has now become somewhat standard in the Section are presented here in order that they might be easily referenced in subsequent articles concerning values measured with this technique.

The experimental setup of the apparatus used in the pulsed-neutron measurements is shown schematically in Figure I-4, the principle elements being a pulsed-neutron generator, a time-base analyzer (multiscaler), a neutron detector, and a solid-state low-noise pulse amplifier and preamplifier. The principal difficulty experienced with this equipment has been noise pickup in the data recording system, primarily due to the electromagnetic field generated by the pulse generator control unit.

A number of system modifications have been tried to eliminate these noise problems, but the least noisy system was obtained using a triaxial

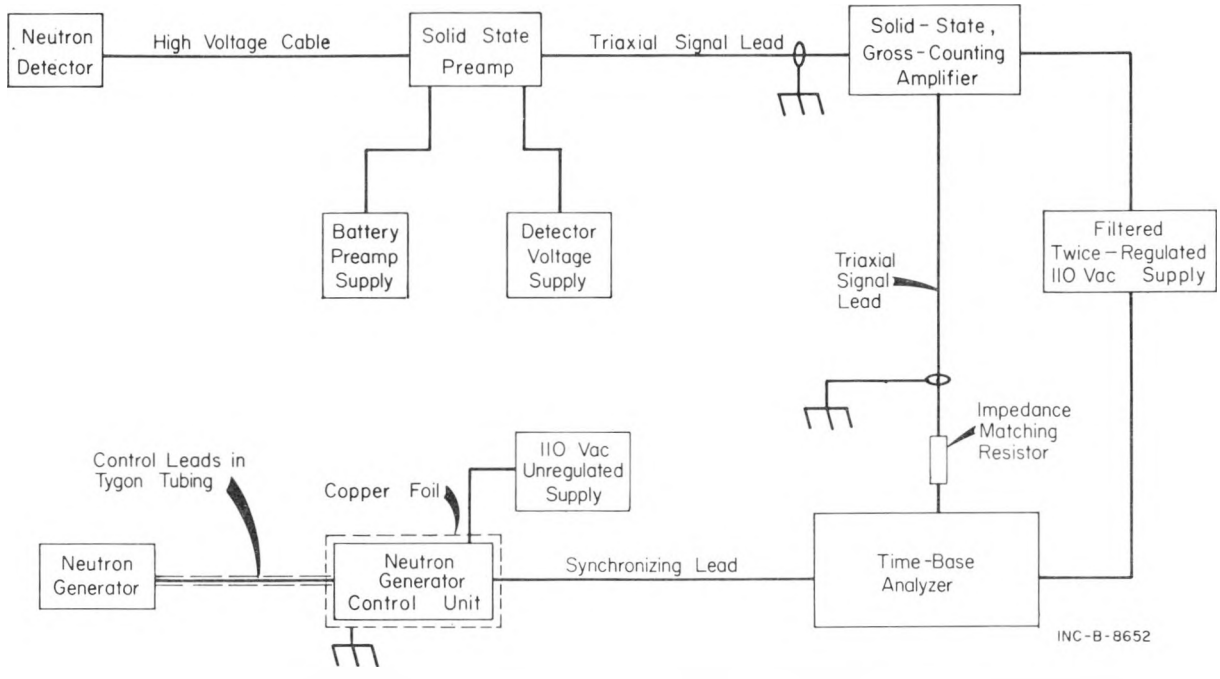

Fig. I-4 Schematic diagram of experimental setup for pulsed-neutron measurements.

signal lead with its outer sheath attached to an earth ground. Also attached to this ground is the entire metal shell housing the time-base analyzer, the metal shell of the amplifier, and the shell of the detector power supply. The entire pulse generator control unit cabinet has been lined with copper foil, and the unit also has been grounded. This control unit is powered from an unregulated 110-V ac line; whereas, the amplifier and time-base analyzer are powered by a doubly regulated and filtered 110-V ac line.

The time-base analyzer, pulse amplifier, and preamplifier were built on-site by the Instrument Development Branch. The analyzer has 512 channels which may be adjusted in width from 100 μsec up to 1.6 sec. Data accumulated are displayed continuously on an attached oscilloscope and may be read out on punched paper tape. This analyzer controls the neutron generator (a standard A-800 Kaman Nuclear neutron-pulse generator) and synchronizes the injection of a neutron pulse with the beginning of an analyzer sweep. The pulse and sweep rate may be varied from 10 per sec to 0.1 per sec in binary increments.

The amplifier used in these experiments is a solid-state, gross-counting amplifier. The output pulse is a constant 8-V amplitude, and the resolving time of the amplifier-preamplifier system is typically 0.5 μsec. The amplifier has a gain-adjust feature, permitting the experimenter to adjust the total gain of the system to suit the experiment. The preamplifier associated with the system is battery powered and has a gain of 25.

The experimental procedure, which has now become nearly standard, requires the analyzer to be set to 100-μsec channel widths with the pulse rate at 10 per sec. With the entire counting system assembled as shown in Figure I-4, a stable reactor period is established, and the amplifier output is recorded with any auxiliary scaler unit. The recorded data are then used to

obtain a resolving time for the system. The detector-neutron generator geometry in the reactor is then established, and a few pulses are fired to adjust the detector position such that the maximum counting rates observed will require resolution corrections less than 10 percent.

With the preliminary adjustments thus completed, the analyzer is set to record reactor background for typically 10^4 sweeps. When this record has been placed on punched paper tape and the analyzer memory cleared, the pulsed-neutron generator is turned on, and the analyzer and pulser are simultaneously started. After sufficient data from the neutron pulse die-away have been recorded to ensure good counting statistics, the pulse generator is turned off, but the analyzer is allowed to continue sweeping until the total number of sweeps equals the number used in the background determination. Typically, the pulse generator is on for 6 minutes, and the analyzer is allowed to sweep for an additional 8 minutes. When the recorded data have been stored on paper tape and the analyzer memory cleared, a second reactor background is taken as before. The data on punched paper tapes for these measurements are then transferred to IBM cards for subsequent computer analysis.

The data obtained above, with the pulse generator in operation, may be described in the form $N(t) = N_p(t) + N_o + B$ where the recorded counts, N(t), are the sum of the rise and decay of the prompt neutron distribution, $N_p(t)$, a delay neutron equilibrium, N_o, due to the rapid pulse rate, and the reactor background, B. The last term, B, is removed from the data by subtracting the average of the two backgrounds obtained above from N(t).

The experimental data are analyzed by IBM-7040 program, GRIPE II, PPCo. 40.0564. This program orders and resolution-corrects the experimental data, determines N_o, and analyzes the data, $N_p(t)$, to determine a value for α, the decay constant of the prompt neutron distribution. The program then calculates a value for reactivity in dollars from the relationship, $\$ = (\alpha - \alpha_o)/\alpha_o$. In this expression, α_o is the Garelis-Russell constant [7], defined as the root of the equation,

$$\int_o^\infty N_p(t)\, e^{\alpha_o t}\, dt - \int_o^\infty N_p(t)\, dt = \frac{N_o}{R}$$

where R is the pulse repetition rate. The program then outputs all input information, all computed parameters with standard deviations, and x-y plots of the corrected data.

1.5 ATRC Safety Rod Worths Using the Pulsed-Neutron Technique (N.C. Kaufman)

The reactivity worth of the ATRC cadmium safety rods has been measured using the pulsed-neutron technique described in Section 1.4 above. These measurements provide values for the ATRC shutdown margin in three different shim configurations and are summarized in Table I-2.

Pulsed-neutron measurements with the safety rods at several different elevations (Runs 1, 2, 3, 4, and 5 in Table I-2) were obtained to construct a calibration curve for the safety rod worth in order to compare it to a curve previously obtained with the reactor period technique [8]. The calibration curve and this comparison are shown in Figure I-5. The curve, labled "Period Calibration", was obtained for a single safety rod using asymptotic periods

TABLE I-2

PULSED-NEUTRON VALUES FOR THE
ATRC SAFETY ROD WORTHS

Run Number	Core Conditions[a]	Safety Rod Position (inches withdrawn)	Subcritical Reactivity[b] (dollars)
1	Outer shims at 76.8 deg; regulating rods NE4 and SW4 out; all neck shims inserted; six Hf inserts in H-holes	26.99	0.99 ± 0.01
2	Same as Run 1	18.00	3.07 ± 0.05
3	Same as Run 1 except outer shims at 75.3 deg; instrument thimble in E flux trap	18.00	3.08 ± 0.06
4	Same as Run 1	8.99	7.43 ± 0.50
5	Same as Run 3	0.0	8.75 ± 0.31
6	Outer shims at 0 deg; neck shims Nos. 2 through 5 out; No. 6 inserted; No. 1 at 25 in.; four Hf inserts in H-holes	0.0	9.30 ± 0.5
7[c]	Outer shims at 160 deg; neck shims Nos. 1, 2, 5, 6 out; neck shims Nos. 3 and 4 inserted; regulating rods NE4 and SW4 at 36.6 in.; 145.5 g of boron uniformly added to fuel annulus; four Hf inserts in H-holes	0.0	7.27 ± 0.16

[a] In all runs, an instrument thimble was in the center flux trap, and none of the flow tubes contained experiments.

[b] All listed errors are one standard deviation as computed by GRIPE II.

[c] Simulated end-of-cycle in 50-50-50 power split.

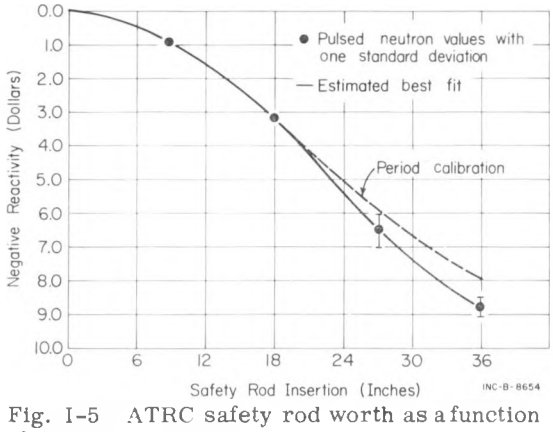

Fig. I-5 ATRC safety rod worth as a function of insertion distance.

and was then normalized to the pulsed-neutron value for a 9-in. insertion for all five safety rods. It may be seen that the values at 18 inches also agree but that below 18 inches, the pulsed neutron values are consistently greater than those predicted from the single rod calibration. This effect has also been observed in ETRC (Section 1.7 below) and is due to the enhancement of the group worth by the vertical flux perturbations associated with the group insertion.

The values reported for Runs 5 and 6 in Table I-2 are in reasonable agreement with previous indications [5] that the safety rod worth changes as the outer shim positions are varied. Additionally, a comparison of the value obtained in Run 5 for a clean reactor in a flat or 50-50-50 power split and the value obtained in Run 7 for a uniformly poisoned, simulated end-of-cycle reactor in a flat power split indicates that the safety rod worth may decrease about 10 percent because of the buildup of fission product poisons during a reactor cycle.

A rather interesting and unexpected sidelight to these measurements was that the value of the Garelis-Russell constant, α_0, remained invariant as the safety rod position was varied within the same shim configuration. This invariance seems somewhat unusual since during the rod-drop measurements, reported in Section 1.3 above, rather significant changes in the radial spatial neutron distribution were detected in the flux traps as the rods inserted. However, the pulsed-neutron and rod-drop reactivity values agree surprisingly well in view of the fundamental difference in the quantity measured. That is, the rod-drop technique determines reactivity from the dynamic response of the reactor following safety rod insertion; whereas, the pulsed-neutron technique determines reactivity in a stable subcritical state.

In the pulsed-neutron measurements, the pulsed-neutron generator was placed on top of the ATRC behind the east flux trap and with a BF_3 detector in the center flux trap in the lower half of the core. The presence of the unused instrument thimble in the east flux trap in Runs 3 and 5 resulted in a value of (ℓ/Λ) that differed slightly from the value of (ℓ/Λ) for the reactor containing only one instrument thimble. This difference was apparently due to a localized influence of the additional instrument thimble, and it necessitated a small correction to the measured reactivities. The reactivities obtained in Runs 3 and 5 were thus multiplied by the ratio of (ℓ/Λ) obtained with two thimbles to (ℓ/Λ) obtained with one thimble. The magnitude of this correction was (130/140), and its applicability is demonstrated by the good agreement between the values reported for Runs 2 and 3 in Table I-2.

1.6 Excess Reactivity in ATR-ATRC 39-kg Core (W. L. Schrader, J. W. Henscheid)

The total reactivity compensation in the ATR can be divided into three parts: (a) the reactivity compensated by the movable shims (neck shims and outer shims), commonly referred to as excess reactivity; (b) the reactivity compensated by the burnable poison (boron in the form of B_4C particles in the fuel plates); and (c) the reactivity compensated by the fixed shims (also called H-hole poison inserts) in the center flux trap baffle. The total reactivity to be compensated is affected by the flux trap experiments and by the desired lobe power distribution [9]. Of particular current interest is the reactivity compensation needed for a core containing no flux trap experiments operating in a nominal 50-50-50 power split or flat power distribution (see Section 1.1 above).

The reactivity compensation in this power split with no experiments has now been measured. A previous measurement of this reactivity was made on the 35-kg core [10], but no attempt was made to maintain a given power distribution. These results were then extrapolated to the 39-kg core with TURBO mockup experiments in the flux traps [9]. Because of the differences between the earlier 35-kg core and the present 39-kg core, it was necessary

to remeasure the reactivity held down by the boron and by the shims. The ATRC core conditions for this measurement were identical to that anticipated for ATR startup. The reactor contained 39-kg of U-235; all flux trap flow tubes contained water; and four hafnium inserts were in the center flux trap baffle (H1, H5, H9, H13).

To permit shim withdrawal beyond the cold, clean critical point, plastic wands containing amorphous natural boron were added stepwise to the water channels of the fuel elements. Simultaneous shim calibrations provided a measurement of the worth of the boron added in each step. In each poison step, the boron wands were inserted in the same water channel in each fuel element to obtain the boron reactivity profile across the fuel annulus as shown in Figure I-6. This profile was then averaged across the fuel annulus to obtain

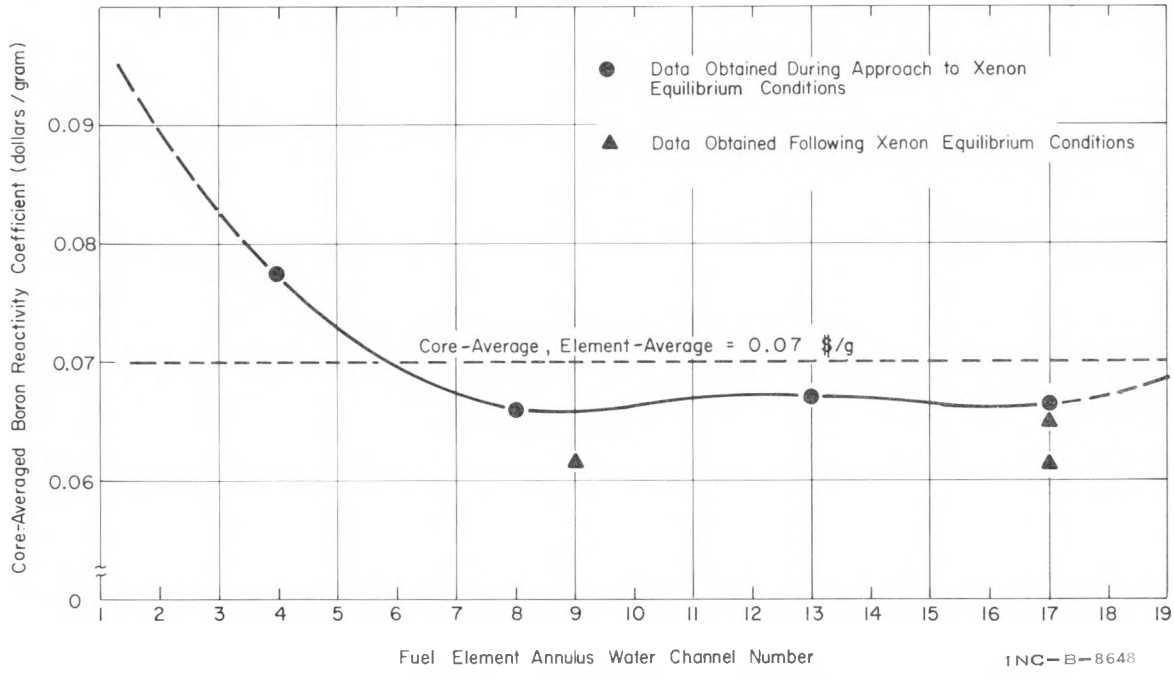

Fig. I-6 Core-averaged boron reactivity profile radially across fuel annulus in ATRC 39-kg core.

a core-averaged, element-averaged boron coefficient of reactivity. The value (11.2$) for the reactivity held down by the burnable poison in the fuel elements is the product of this coefficient and the 160 g of natural boron in the fuel. Points obtained on this profile after reaching simulated xenon equilibrium conditions were not used in the averaging since they were probably influenced by self-shielding.

The excess reactivity held down by the movable shims has been somewhat arbitrarily divided into three parts: (a) that required to compensate for the buildup of equilibrium xenon in the ATR, (b) that required to reach the point in ATR core life at which there is insufficient shimming left to maintain the 50-50-50 power split, and (c) that held down by the shims remaining in the core after the 50-50-50 power split can no longer be maintained. These partial excess reactivities, obtained by summing the reactivity increments of the poisoning sequence, along with the corresponding shim configurations are shown in Table I-3. The sum of all reactivity increments (11.3$) is the total excess reactivity held down by the movable shims. This is nearly equal to

TABLE I-3

EXCESS REACTIVITIES AND SHIM CONFIGURATIONS IN ATR-ATRC 39-kg CORE

Core Conditions	Shim Configuration		Excess Reactivity of Step[a]
	Outer Shims	Neck Shims	
Cold, clean	All at 77.5 deg	NE4 and SW4 withdrawn; all others inserted	0
Xenon equilibrium conditions in 50-50-50 power split	All at 106 deg	All No. 1 and No. 6 shims and NE4 and SW4 withdrawn; all others inserted	5.1 ± 0.1$
End of 50-50-50 power split	All at 160 deg	All No. 3 shims inserted; NE4 and SW4 at 39 in.; all others withdrawn	4.5 ± 0.1$
All shims withdrawn	All at 160 deg	All withdrawn	1.7 ± 0.05$
		Total	11.3 ± 0.2$

[a] Error limits are estimates of one standard deviation based primarily on uncertainties in the shim calibrations.

the 11.2$ held down by the burnable poison. The four fixed shims in the center flux trap baffle held down an additional 1.5$.

1.7 ETRC Safety Rod Worths with Pulsed-Neutron Technique (N. C. Kaufman, R. J. Forrester, R. L. Copyak)

Pulsed-neutron measurements were made in ETRC to measure the reactivity worth of the four safety rods with the reactor core in a mock-up of ETR Cycle 73. Data were taken with the reactor subcritical at five positions of safety rod insertion. In this manner, it was possible to obtain not only total safety rod worth but to construct an integral safety rod worth curve to compare with the ETRC standard rod calibration curve.

The results, shown in Figure I-7, indicated a total safety rod worth of 8.6 ± 0.5$ for the Cycle 73 ETRC mock-up. The curve in Figure I-7, labeled "ETRC Standard Curve", was obtained by normalizing the ETRC standard rod calibration curve (obtained by measuring reactor periods during a uniform poison experiment and subsequent use of the Inhour equation) to the pulsed-neutron value at 7 in. of insertion. The measured values at 14 in. and 18 in. insertion may be seen to coincide with this normalized curve at those points; although below 18 in., the measured values were greater than the values on this curve. This difference toward the safety rod lower limits is to be expected since the ETRC standard curve is based on the worth of a single rod. It will, thus, underestimate the worth of the four rods due to the vertical flux perturbations produced as the larger number of rods is inserted.

In addition to the measurements described above, an experiment was done to determine whether the measured values were dependent on the geometrical

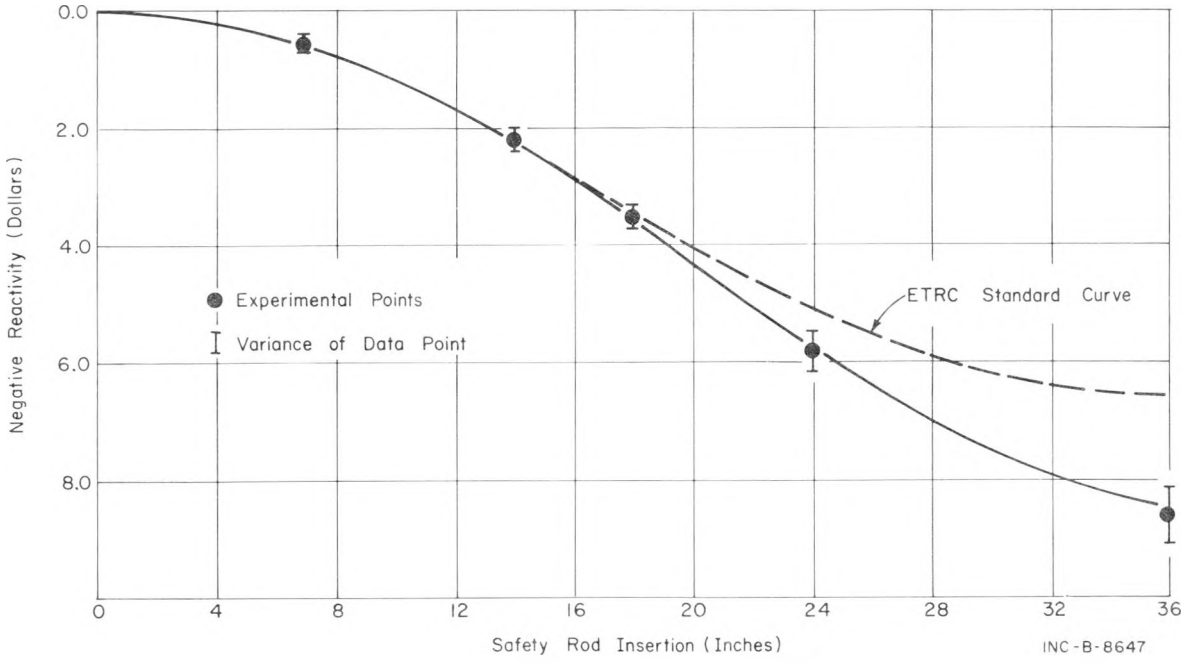

Fig. I-7 ETRC safety rod worth as a function of insertion distance.

arrangement of the pulsed-neutron generator and the BF_3 detector used. Measurements were made with the safety rods at 7-, 14-, and 18-in. insertion in two geometries: the generator and detector at opposite extremities of the NW - SE diagonal of the reactor and of the NE - SW diagonal, the data in Figure I-7 being from the latter. Within the experimental uncertainty, no differences in the measured values were detected.

These measurements were performed using the procedure described in Section 1.4 above. However, at the time they were done, some rather severe difficulties were experienced with electronic noise in the first several data channels. This noise precluded a Garelis-Russell analysis although α, the decay constant of the prompt fundamental mode, could be obtained. In order to calculate reactivity, the relationship, $\$ = (\alpha - c)/c$, was used where c was taken as the value of β/ℓ measured for ETRC in an autocorrelation experiment. The value used ($c = 131.0$) is not expected to differ from the Garelis-Russell constant, usually employed in this relationship, by more than 4 percent at the safety rod lower limit and should differ even less for the other data points.

2. ENGINEERING EXPERIMENTS
(V. A. Walker)

2.1 ATR Fuel Element Procurement (M. L. Griebenow, G. N. Fillmore, J. A. Hendricks)

The contract for the first fully enriched ATR fuel assemblies was awarded July 30, 1964. The contract covered 240 assemblies and was completed with the final shipment on June 27, 1966. The first 42 assemblies received were not considered satisfactory for full-power operation but were accepted for ATRC

use. With the exception of one loose plate assembly, the remaining assemblies received have been dimensionally and visually inspected. This inspection detected one assembly with a cracked upper end fitting (in the upper end of the handling tool hole) that was returned to the fabricator for a new end fitting. One other assembly inadvertently contained a fuel plate with fuel run out at the upper end, resulting in a small area of fuel contained in the upper comb area. Since the fuel was in an area of low heat flux and minimum coolant temperature and did not approach within 3/32 of the pinhole, it was felt that the assembly could perform satisfactorily in selected positions.

Forty-three of the one hundred and seventy assemblies scheduled for high-power ATR usage have successfully withstood hydraulic testing at 120 percent of full flow at 350°F. These assemblies have been machined where required to allow reactor insertion; the combs have been tack welded; and the assemblies are ready for Core I loading. However, because of deviations from the mechanical tolerence specifications in critical regions, seven assemblies will be placed in the core positions with lower power generation rates. The remaining 127 assemblies will be given a hydraulic test before insertion in ATR.

As a means of checking quality control and to assist in statistical hot spot - hot channel analysis, the channel spacing of all 170 assemblies scheduled for high-power ATR operation has been plotted. The distribution of the channel average spacing is shown in Figure I-8 for Planes A and C (3/8 inch from each side plate) and in Figure I-9 for Plane B (within 3/8 inch of the center of the plate span). The distribution about the average is shown in Figures I-10 and -11 for Planes A and C and for Plane B, respectively. It is apparent that the average channel spacing is distributed 0.0015 to 0.002 inch above the nominal 0.078-inch spacing. The fact that the deviation from average was maintained better at Plane B than at Planes A and C where the fuel plates were supported suggests extensive use of a straightening procedure on the assembled units. The channel spacing does not fall within the predicted distribution used in hot spot - hot channel analysis to date. The assemblies to be used in the hot core positions must be handpicked to maintain the safety margins previously reported [11].

2.2 ATR Graded Fuel 7F Designation (M. L. Griebenow, G. N. Fillmore, C. A. Moore)

The possibility of radially varying the fuel content in the assemblies operating in the hot ATR core positions has been investigated [12]. The potential reduction in peak heat fluxes, oxidation rates, and subsequent thermal stresses would allow higher power operation with the same operating confidence level. The 7F graded fuel loading employs a maximum of three fuel and three boron densities. The fuel and boron contents, as compared to the MARK IV assembly, are shown in Table I-4. The lobe positions in which the 7F assemblies would be used are shown in Figure I-12. The three fuel and boron densities allow a reasonable approach to the optimum radial graduation, and it is felt that the added expense of additional density variation could not be justified by the small potential gain in performance.

The flux data for the quarter-core model, shown in Figure I-12, was computed as a function of time during the 17-day cycle using the TURBO [13] code on an IBM-7040. All thermal-hydraulic and corrosion calculations were performed

using the MACABRE [14] code and a modified PDQ [a] code. The PDQ code solved the azimuthal heat conduction.

The core loading was analyzed in unbalanced (40-50-60 MW/lobe) 250-MW operation at the nominal and at the 2σ level; the latter was determined by what is believed to be a conservative analysis of the manufacturing tolerences and operating uncertainties. The factors used are listed in Table I-5. A comparison of 7F with the MARK IV operating parameters, computed on a similar basis, is shown in Table I-6. In the 7F assembly, the most critical stresses will develop in Plate 15. The 2σ calculations produced the greatest stress level at the end of the cycle when the oxide layer was at a maximum; but because the effect of burnup exceeded the effect of oxidation, the largest stresses in the nominal case were produced after only 12 days of operation. The computed temperatures and stresses for the most critical location are shown in Figures I-13 through -16. Because the ability of the 7F fuel assembly to withstand the stresses developed at the 250 MW (the 2σ level was questionable), the 2σ calculations were repeated (again in the unbalanced configuration) at 208 MW. This power has a 50-MW hot lobe. The operating parameters at this power level are also shown in Table I-6. The computed temperatures and stresses are shown in Figures I-17 and -18.

The behavior of a fuel plate with portions operating beyond the yield stress, as in the 2σ-250 MW case, is not well understood. Recent experimental stress analysis at the NRTS indicates that relatively large areas of a fuel plate may exceed the yield stress without the production of destructive buckling. Further tests, now underway, are designed to determine the ability of the 7F loading to operate at an unbalanced (40-50-60 MW/lobe) 250-MW power level.

---

[a] As yet unreported.

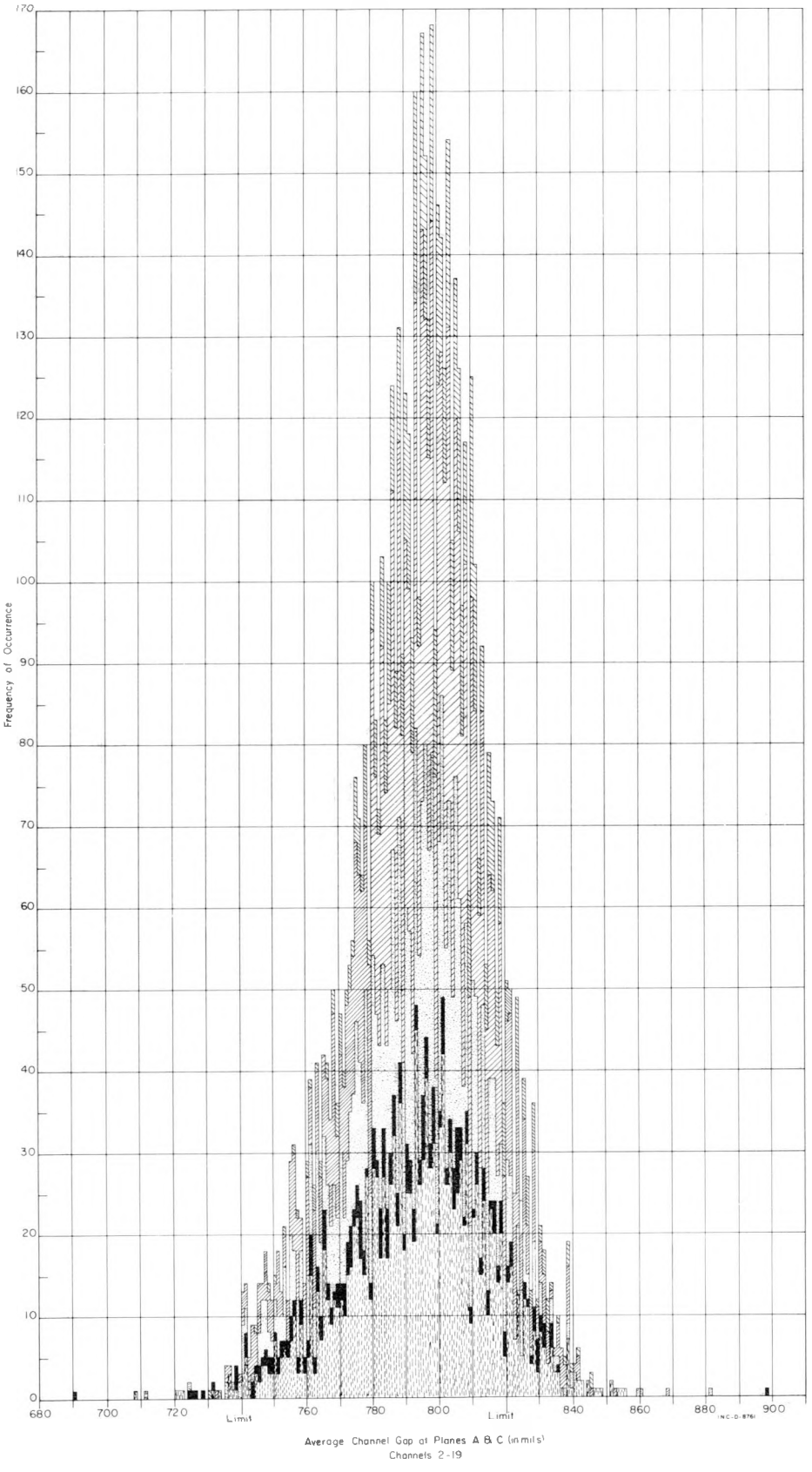

Fig. I-8 Average channel gap at Planes A and C.

A 47C
A 48C
A 49C
A 50C
A 51C
A 52C
A 53C
A 54C
A 55C
A 56C
A 57C
A 58C
A 59C
A 68C
A 70C
A 71C
A 72C
A 73C
A 76C
A 77C
A 25C
A 60C
A 74C
A 75C
A 78C
A 80C
A 81C
A 82C
A 83C
A 84C
A 85C
A 86C
A 88C
A 89C
A 90C
A 91C
A 92C
A 95C
A 96C
A 97C
A 98C
A 99C

A 61C
A 65C
A 79C
A 93C
A100C
A101C
A102C
A103C

A 63C
A104C
A105C
A106C
A107C
A108C
A109C
A110C
A111C
A112C
A113C
A114C
A115C
A116C
A117C
A118C
A119C
A121C
A126C
A 94C
A123C
A127C
A128C
A131C
A133C
A134C
A138C
A139C
A140C
A141C
A142C
A143C
A144C
A146C
A148C
A149C
A152C

A 62C
A 64C
A 67C
A120C
A122C
A124C
A125C
A130C
A132C
A135C
A136C
A137C
A145C
A147C
A150C
A151C
A153C
A154C
A155C
A156C
A157C
A158C
A159C
A160C
A161C
A162C
A163C
A164C
A165C
A166C
A168C
A169C
A170C
A172C
A173C
A174C
A175C
A176C
A177C
A178C
A179C
A180C
A182C
A183C
A184C
A185C
A186C
A187C
A188C
A189C
A190C
A191C
A192C
A193C
A194C
A196C
A197C
A198C
A199C
A200C

A 69C
A129C
A171C
A195C
A201C
A202C
A203C
A 66C
A 87C
A167C
A181C
A204C
A205C
A206C
A207C
A208C
A209C
A210C
A211C
A212C

FIG. 1-8. LEGEND

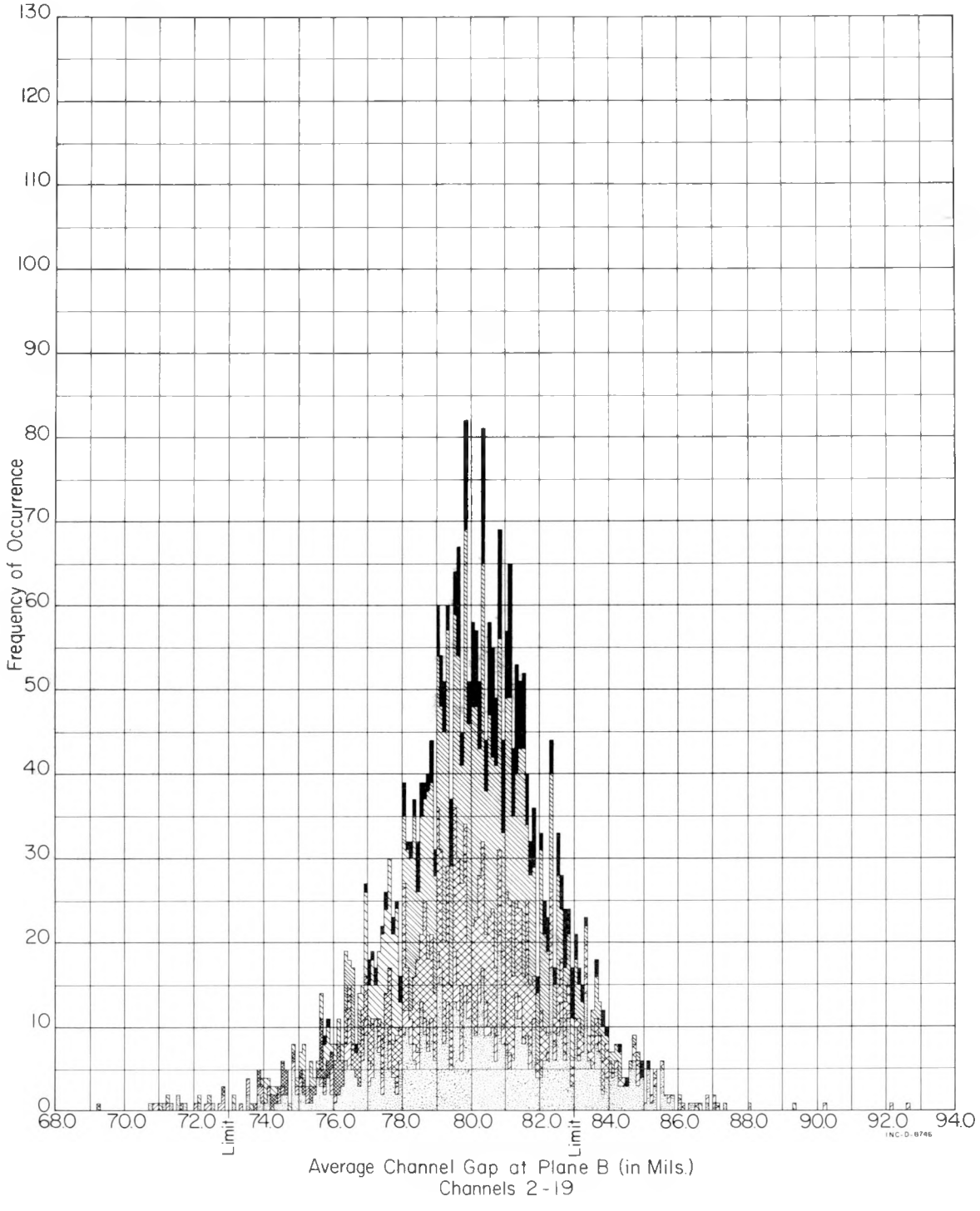

Fig. I-9 Average channel gap at Plane B.

A 47C
A 48C
A 49C
A 50C
A 51C
A 52C
A 53C
A 54C
A 55C
A 56C
A 57C
A 58C
A 59C
A 68C
A 70C
A 71C
A 72C
A 73C
A 76C
A 77C
A 25C
A 60C
A 74C
A 75C
A 78C
A 80C
A 81C
A 82C
A 83C
A 84C
A 85C
A 86C
A 88C
A 89C
A 90C
A 91C
A 92C
A 95C
A 96C
A 97C
A 98C
A 99C

A 61C
A 65C
A 79C
A 93C
A100C
A101C
A102C
A103C

A 63C
A104C
A105C
A106C
A107C
A108C
A109C
A110C
A111C
A112C
A113C
A114C
A115C
A116C
A117C
A118C
A119C
A121C
A126C
A 94C
A123C
A127C
A128C
A131C
A133C
A134C
A138C
A139C
A140C
A141C
A142C
A143C
A144C
A146C
A148C
A149C
A152C

A 62C
A 64C
A 67C
A120C
A122C
A124C
A125C
A130C
A132C
A135C
A136C
A137C
A145C
A147C
A150C
A151C
A153C
A154C
A155C
A156C
A157C
A158C
A159C
A160C
A161C
A162C
A163C
A164C
A165C
A166C
A168C
A169C
A170C
A172C
A173C
A174C
A175C
A176C
A177C
A178C
A179C
A180C
A182C
A183C
A184C
A185C
A186C
A187C
A188C
A189C
A190C
A191C
A192C
A193C
A194C
A196C
A197C
A198C
A199C
A200C

A 69C
A129C
A171C
A195C
A201C
A202C
A203C
A 66C
A 87C
A167C
A181C
A204C
A205C
A206C
A207C
A208C
A209C
A210C
A211C
A212C

FIG. I-9 LEGEND

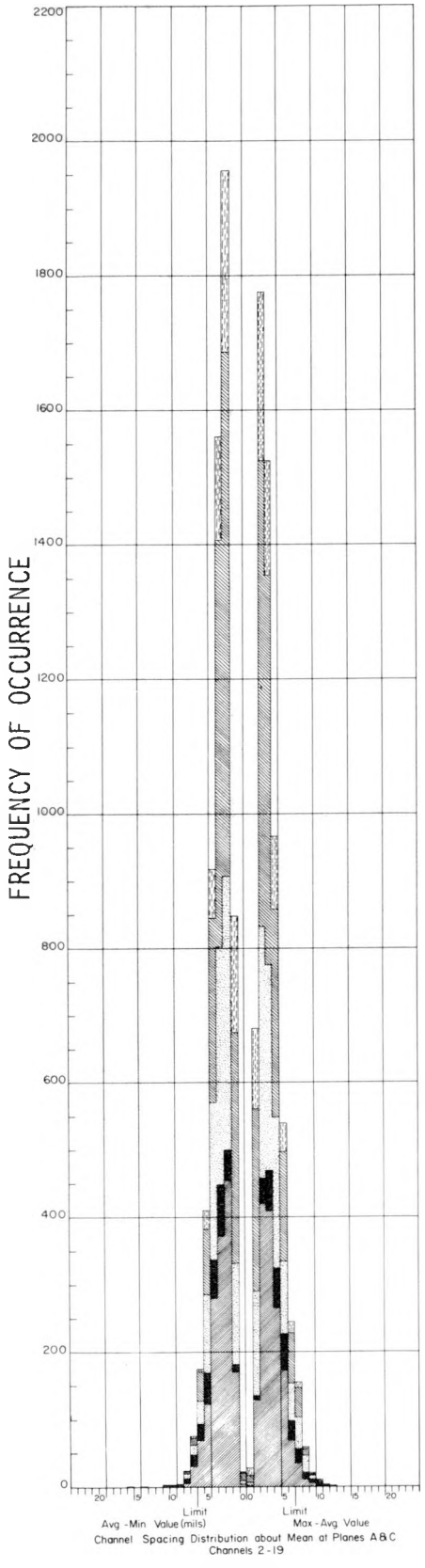

Fig. I-10 Channel spacing distribution about the average at Planes A and C.

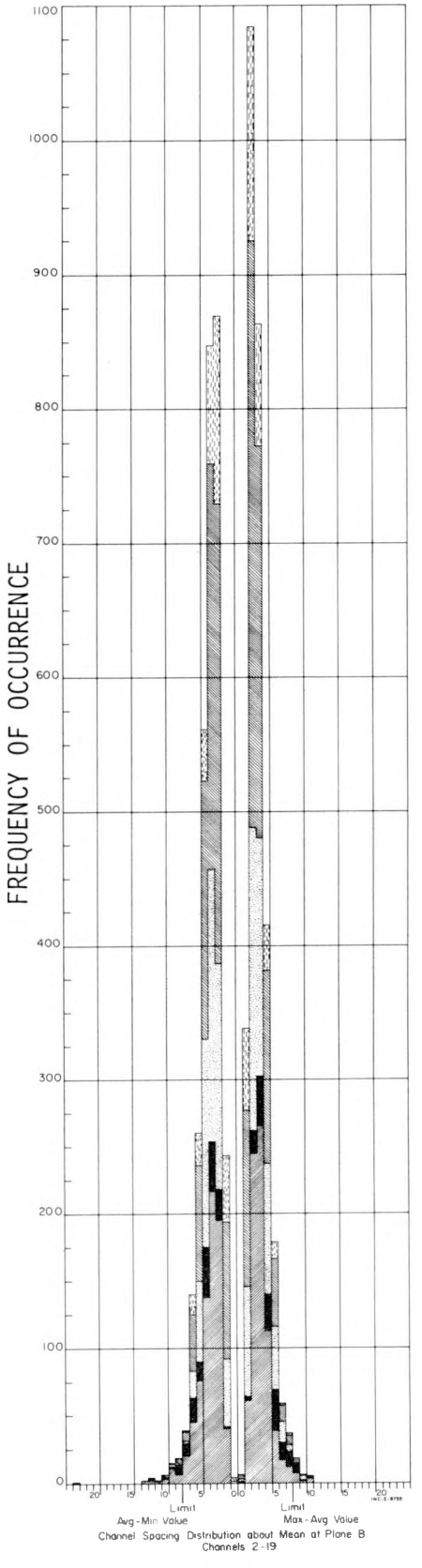

Fig. I-11 Channel spacing distribution about the average at Plane B.

A 47C
A 48C
A 49C
A 50C
A 51C
A 52C
A 53C
A 54C
A 55C
A 56C
A 57C
A 58C
A 59C
A 68C
A 70C
A 71C
A 72C
A 73C
A 76C
A 77C
A 25C
A 60C
A 74C
A 75C
A 78C
A 80C
A 81C
A 82C
A 83C
A 84C
A 85C
A 86C
A 88C
A 89C
A 90C
A 91C
A 92C
A 95C
A 96C
A 97C
A 98C
A 99C

A 61C
A 65C
A 79C
A 93C
A100C
A101C
A102C
A103C

A 63C
A104C
A105C
A106C
A107C
A108C
A109C
A110C
A111C
A112C
A113C
A114C
A115C
A116C
A117C
A118C
A119C
A121C
A126C
A 94C
A123C
A127C
A128C
A131C
A133C
A134C
A138C
A139C
A140C
A141C
A142C
A143C
A144C
A146C
A148C
A149C
A152C

A 62C
A 64C
A 67C
A120C
A122C
A124C
A125C
A130C
A132C
A135C
A136C
A137C
A145C
A147C
A150C
A151C
A153C
A154C
A155C
A156C
A157C
A158C
A159C
A160C
A161C
A162C
A163C
A164C
A165C
A166C
A168C
A169C
A170C
A172C
A173C
A174C
A175C
A176C
A177C
A178C
A179C
A180C
A182C
A183C
A184C
A185C
A186C
A187C
A188C
A189C
A190C
A191C
A192C
A193C
A194C
A196C
A197C
A198C
A199C
A200C

A 69C
A129C
A171C
A195C
A201C
A202C
A203C
A 66C
A 87C
A167C
A181C
A204C
A205C
A206C
A207C
A208C
A209C
A210C
A211C
A212C

FIGS. I-10 AND I-11 LEGEND

TABLE I-4

STANDARD ATR MARK IV AND
RADIAL ZONE-LOADED FUEL DISTRIBUTION

Fuel Type	Plates	U-235 Content[a] (volume percent)	B-10 Content[a] (volume percent)
Mark IV (975-g fuel)	1-19	100	100
Fuel -- 7F (1075-g fuel)	1-2, 18-19	80	274
	3-4, 16-17	101	147
	5-15	122	21

[a] Both values of content are based on the volume percent of U-235 and B-10 in the Mark IV being 100 volume percent.

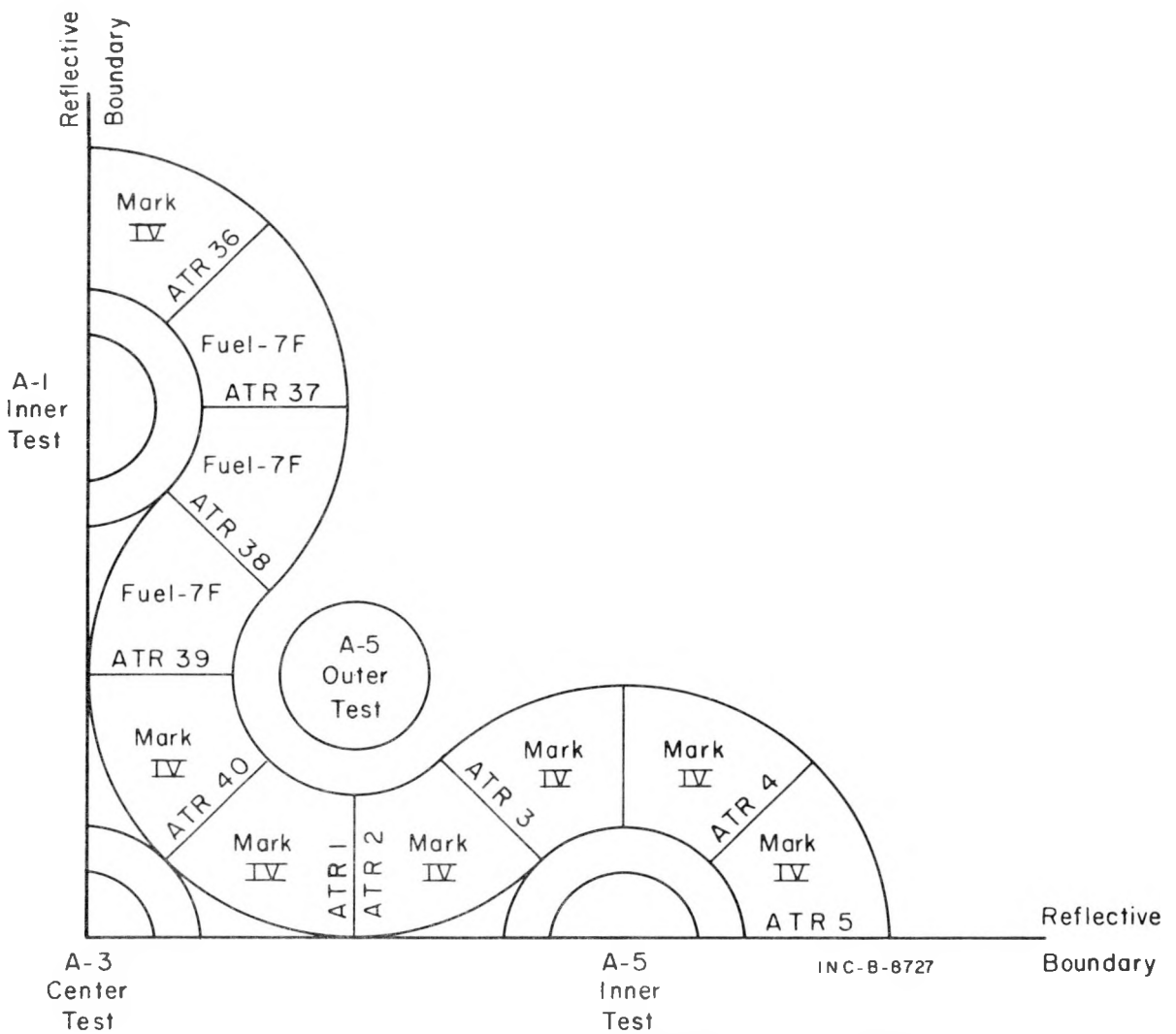

Fig. I-12 The ATR one-fourth core model for TURBO calculations.

TABLE I-5

2σ HOT SPOT - HOT CHANNEL FACTORS

Heat Flux Factors	
Power Measurement and Control	1.05
Fuel Content -- Local	1.08
Fuel Core Area	1.04
ATR-ATRC Correspondence	1.05
Product	1.238
Hot Channel Factors	
Coolant Channel Geometry	1.084
Fuel Content -- Hot Track	1.03
Flow Distribution -- External Effects	1.05
Power Measurement and Control	1.05
Fuel per Plate	1.01
Transverse Velocity Variation	1.00
ATR-ATRC Correspondence	1.05
Product	1.305
Heat Transfer Coefficient Factors	
Safety Factor	0.8
Velocity and Hydraulic Diameter Effect[a]	0.897
Product	0.718

[a] 0.073-inch channel average with a dimple to 0.080 inch at the hot spot.

TABLE I-6

CALCULATED OPERATING PARAMETERS

	Reference MARK IV Assembly		7-F Assembly	
	Balanced 250 MW	Unbalanced 250 MW	Unbalanced 208 MW	Unbalanced 250 MW
Hot Plate:	19	19	5	5
Maximum Nominal BOL Temperature (°F)	307	345	---	331
2σ Maximum BOL Temperature (°F)	360	428	365	404
Maximum Nominal Temperature During Cycle (°F) (days)	333 (17)	431 (17)	---	372 (12)
2σ Maximum Temperature During Cycle (°F) (days)	470 (17)	758 (17)	444 (17)	562 (17)
Oxide Thickness at Nominal Hot Spot (mils)	0.66	1.17	---	0.84
Oxide Thickness at 2σ Hot Spot (mils)	1.64	3.32	1.38	2.08
Plate with Maximum Thermal Stress:	18	18	15	15
Maximum Nominal BOL Temperature (°F)	307	345	---	324
2σ Maximum BOL Temperature (°F)	358	423	357	396
Maximum Nominal Temperature During Cycle (°F) (days)	333 (17)	426 (17)	---	357 (12)
2σ Maximum Temperature During Cycle (°F) (days)	455 (17)	713 (17)	442 (17)	542 (17)
Oxide Thickness at Nominal Hot Spot (mils)	0.66	1.17	---	0.82
Oxide Thickness at 2σ Hot Spot (mils)	1.52	3.06	1.34	2.01

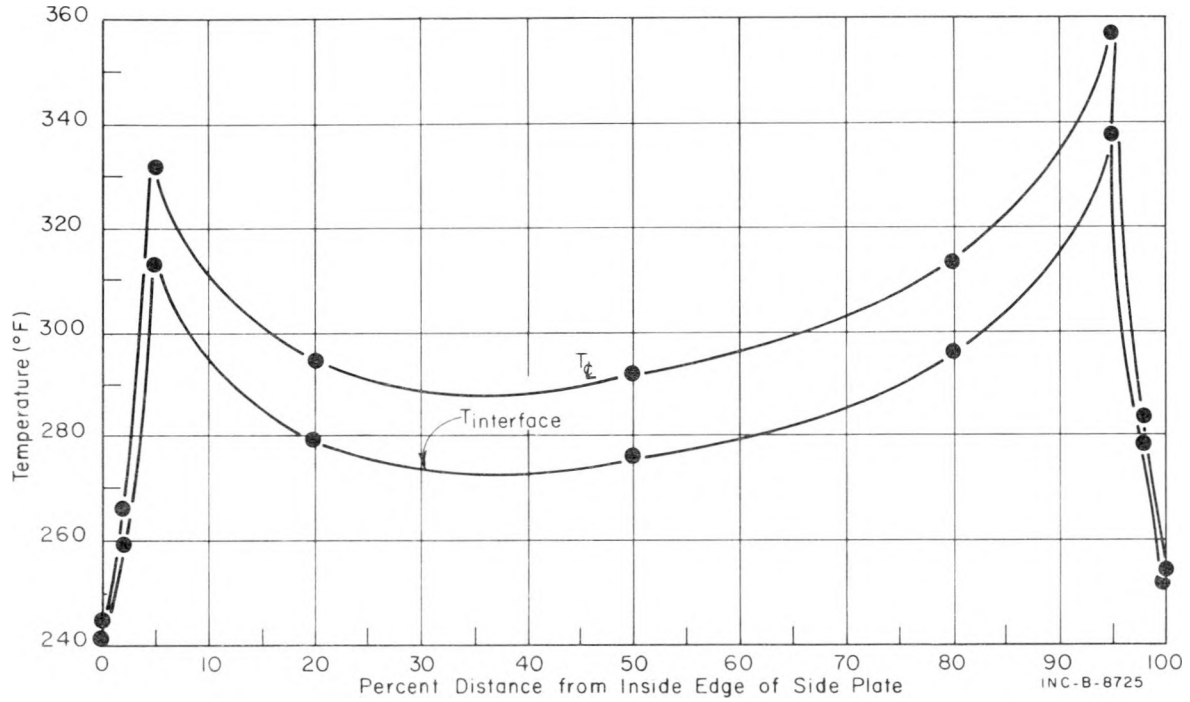

Fig. I-13 Nominal, 250-MW (60-MW lobe), 12-day, oxide-aluminum interface and plate centerline temperature for Plate 15, 30 inches from top.

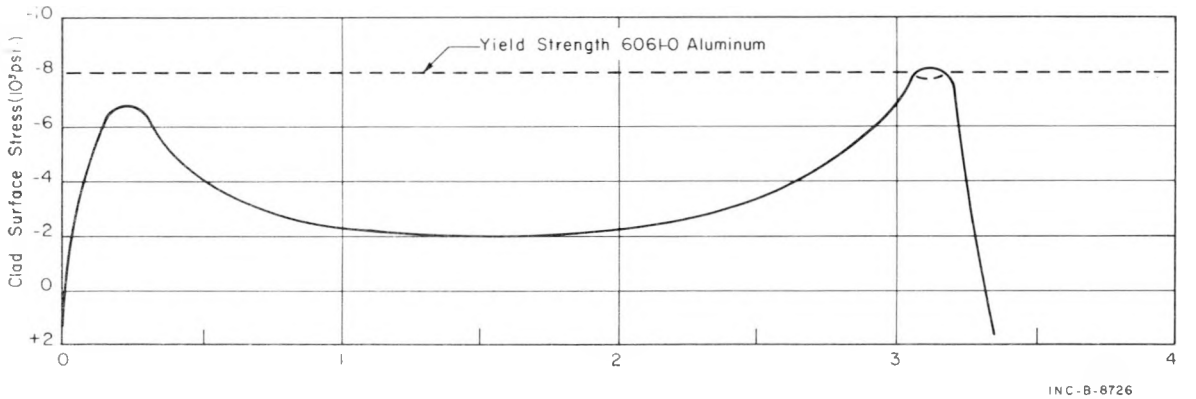

Fig. I-14 Clad surface stress and yield strength corresponding to conditions shown in Figure I-13.

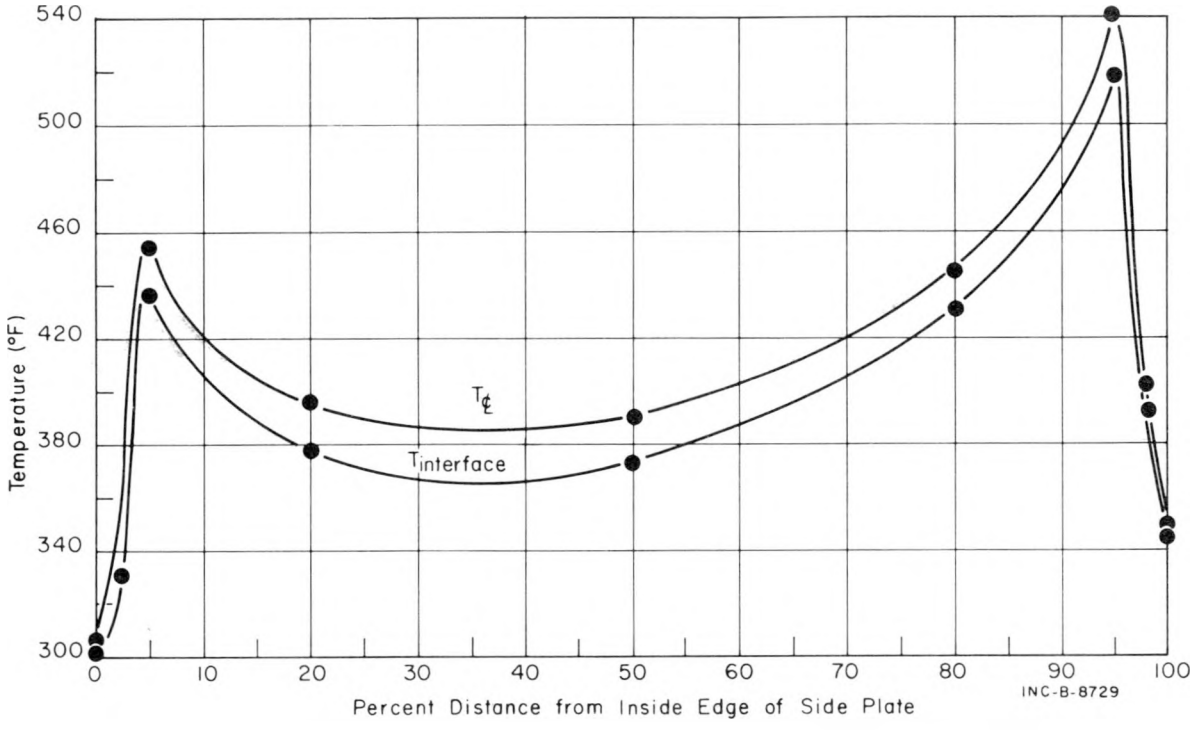

Fig. I-15 2σ maximum, 250-MW (60-MW lobe), end of cycle, oxide-aluminum interface and plate center-line temperature for Plate 15, 30 inches from top.

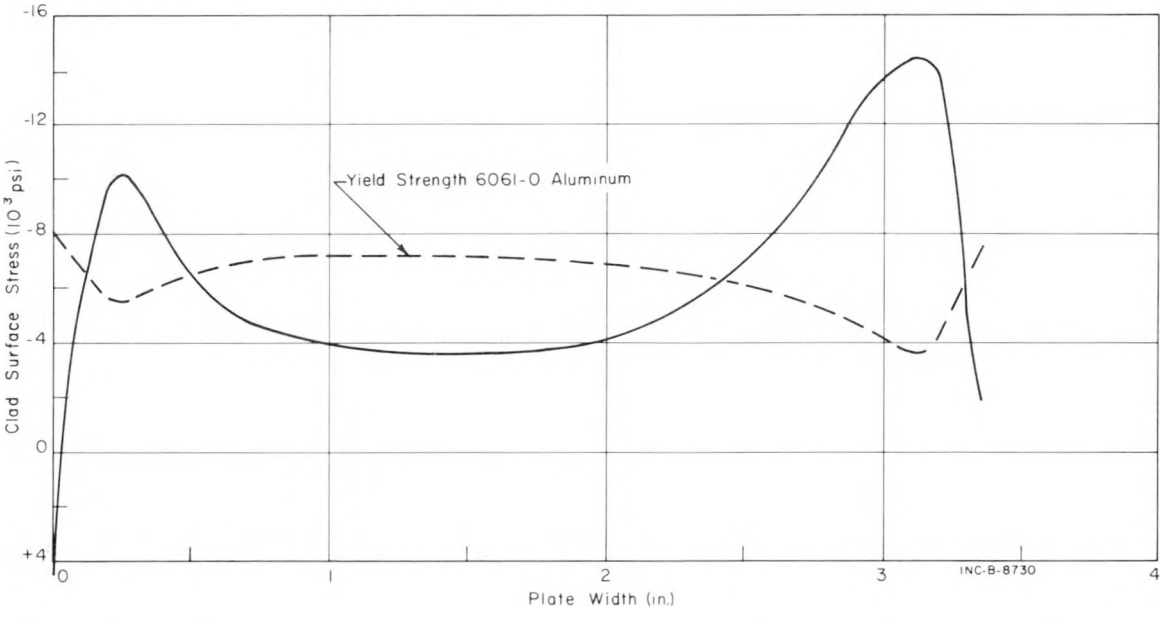

Fig. I-16 Clad surface stress and yield strength corresponding to condition shown in Figure I-15.

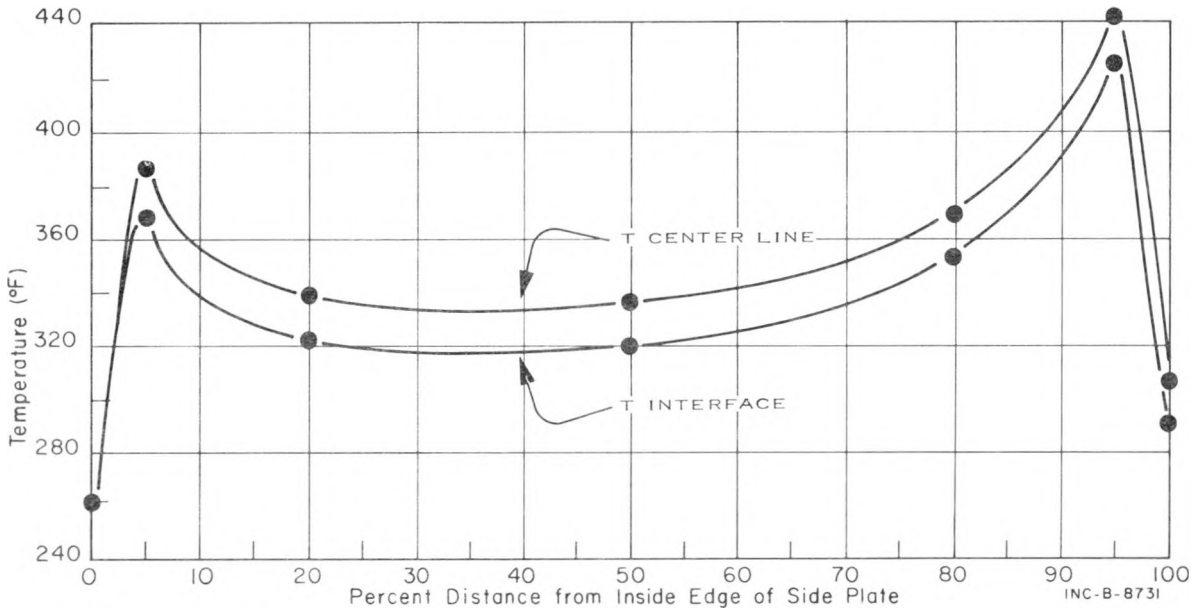

Fig. I-17 2σ maximum, 208-MW (50-MW lobe), end of cycle, oxide-aluminum interface and plate center-line temperature for Plate 15, 28 inches from top.

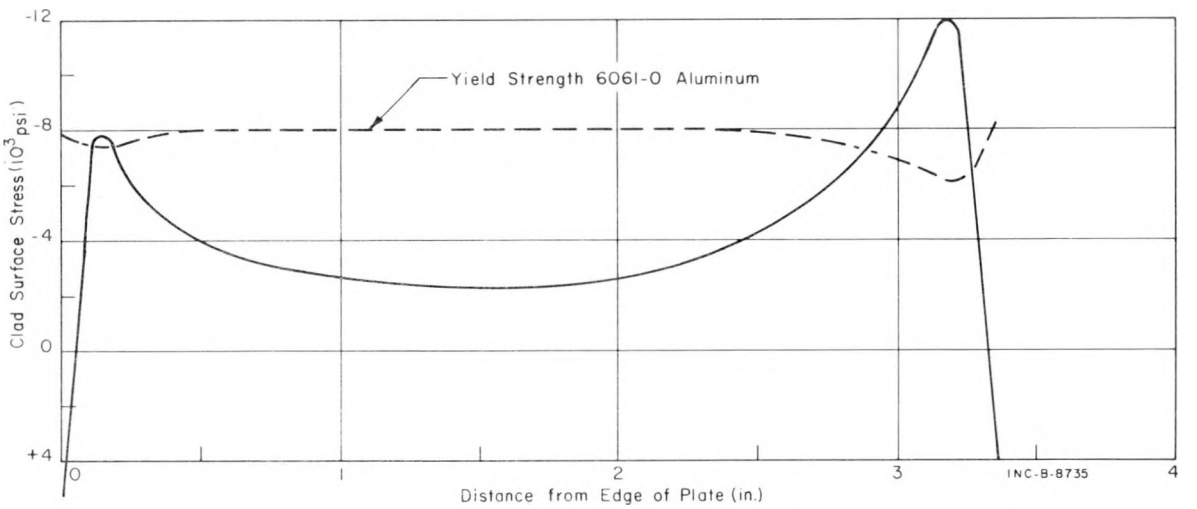

Fig. I-18 Clad surface stress and yield strength corresponding to conditions shown in Figure I-17.

3. METALLURGICAL DEVELOPMENT
(G. W. Gibson)

3.1 Compatibility Studies (K. C. Sumpter, R. J. Pollard, B. G. Carlson, W. Ryder [a], E. S. Bell [a])

In an endeavor to establish test fuel plate fabrication criteria, employing UAl_x dispersion with Ni, Cr, and Nb, several feasibility experiments were conducted using powder metallurgy techniques. Basically, the experiments consisted of blending -100+200 mesh, UAl_x powder with -200 mesh metal for 4 hours, compacting the blended materials at 93 tsi, and sintering for 2 hours in hydrogen or helium. The sintering temperature was determined by the temperature necessary for fabricating test fuel plates. Table I-7 depicts the

TABLE I-7

THERMAL COMPATIBILITY OF UAl_x WITH VARIOUS METALS

Material and Sample Number	Atmosphere	Temperature (°C)	X-Ray Diffraction Results
Ni-UAl_3 1221	H_2	800	UAl_2, Ni major specie; UAl_3, UO_2 unidentifiable minor specie
Ni-UAl_3 1222	H_2	1000	Unidentifiable major specie; UAl_2, Ni minor specie
Ni-UAl_3 1223	H_2	1200	Unidentifiable major specie; Ni minor specie
Cr-UAl_3 1224	H_2	800	UAl_3, UAl_2, Cr major specie; unidentifiable minor specie
Cr-UAl_3 1225	H_2	1000	UAl_2 major specie; complex phases unidentifiable
Cr-UAl_3 1226	H_2	1200	Complex phases unidentifiable; minor specie UAl_2
Nb-UAl_3 1258	H_2	800	UAl_2, UAl_3, Nb major specie
Nb-UAl_3 1260	H_2	1000	Not performed
Nb-UAl_3 1262	H_2	1200	UAl_2, Nb major specie; AlNb minor specie
Nb-UAl_3 1257	He	800	Not performed
Nb-UAl_3 1259	He	1000	Not performed
Nb-UAl_3 1261	He	1200	UAl_2, Nb major specie; AlNb minor specie

[a] Analytical Chemistry Branch.

sample composition, test conditions, and X-ray diffraction results. Because of the complexity of these systems and the lack of available standards, some phases were not identifiable by diffraction techniques. Microprobe studies were conducted on some of the samples, and the results are discussed in the next section of this report.

Figure I-19 shows the Ni and Cr compacts after sintering at 800, 1000, and 1200°C temperatures. It is apparent that the Ni underwent severe reaction at 1200°C and somewhat less reaction at 1000°C with the UAl_x. Figure I-20 depicts the microstructure of the Ni-UAl3 samples. In an attempt to identify the complex structure of the 1200°C sample, photomicrographs were taken at 1000X as indicated in Figure I-21. The eutectic area bears a remarkable resemblance to Al-Al_3Ni structures, exhibiting both blade- and needle-like whiskers.

Neither the Cr nor Nb sintered as well as the Ni samples; however, reaction between these metals and UAl_3 is readily apparent as shown in Figures I-22 and I-23. It is difficult to draw significant conclusions at this early date, but the trend seems to be, with the metals investigated, that UAl_3 is compatible up to 800°C. Further studies are underway to determine what can be done to inhibit these reactions at the higher temperatures.

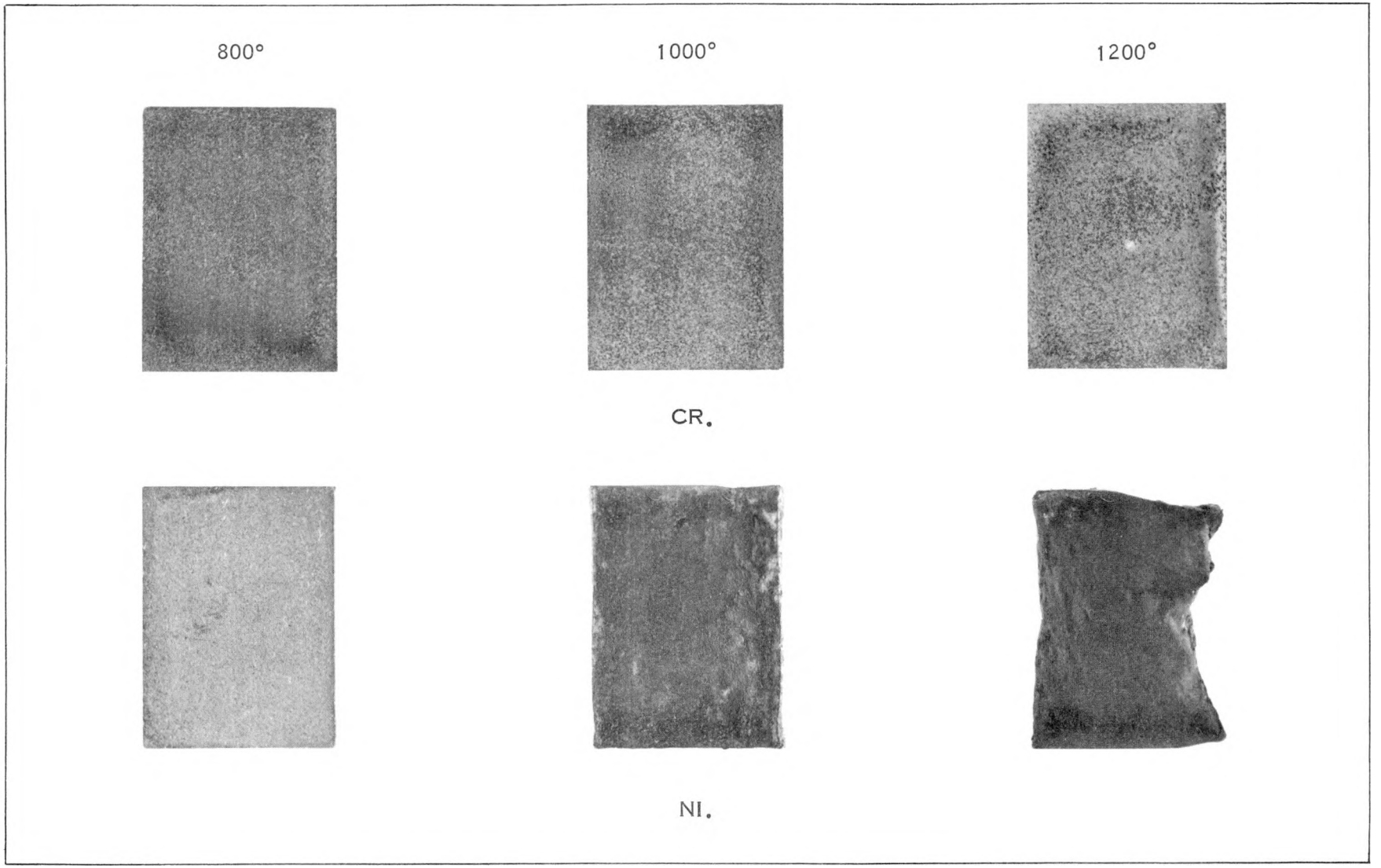

Fig. I-19 Ni and Cr-UAl_3 compacts after sintering for 2 hours in H_2 (temperatures in °C).

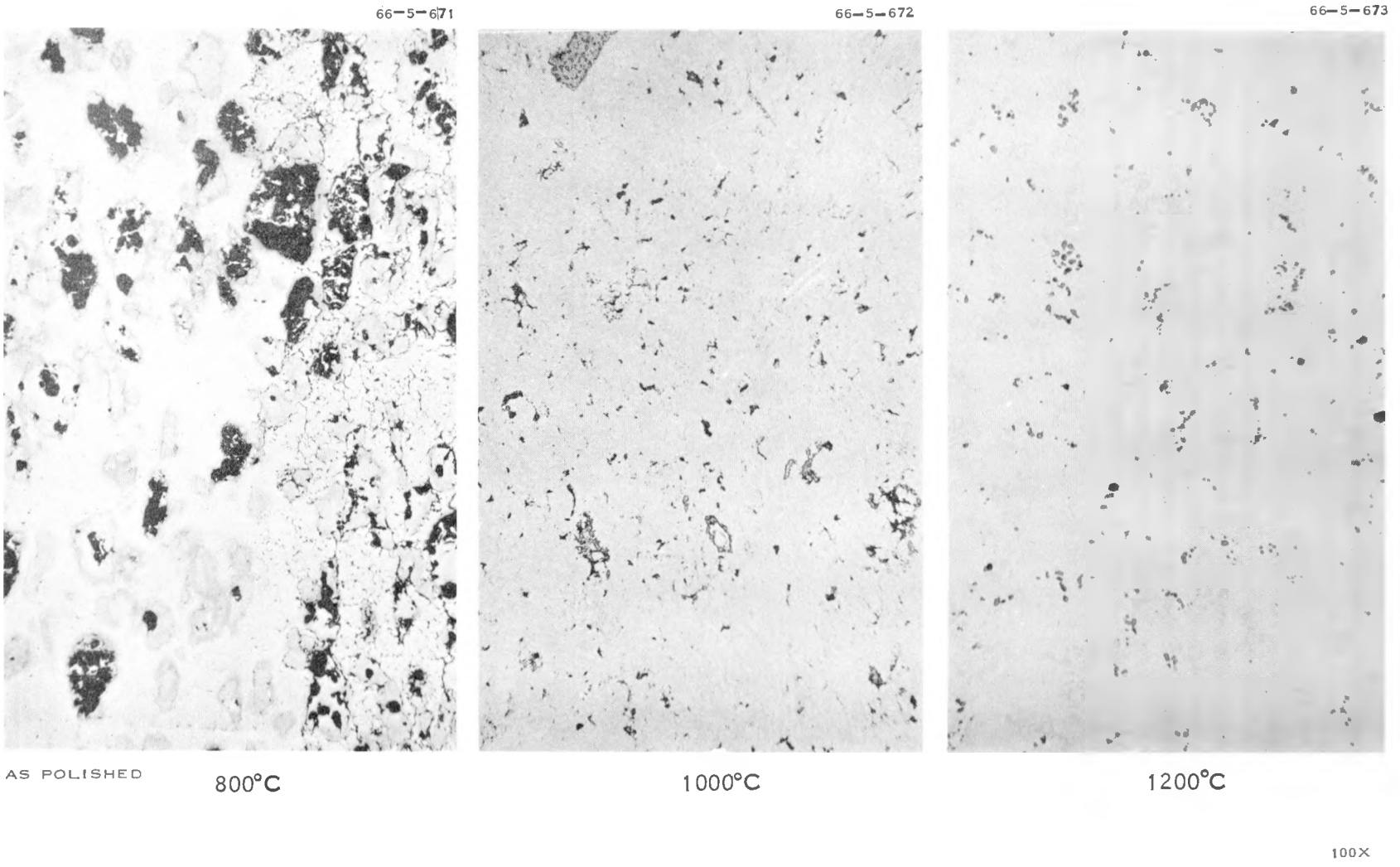

Fig. I-20 Microstructure of Ni-UAl_3 samples, sintered in H_2 at the temperatures indicated.

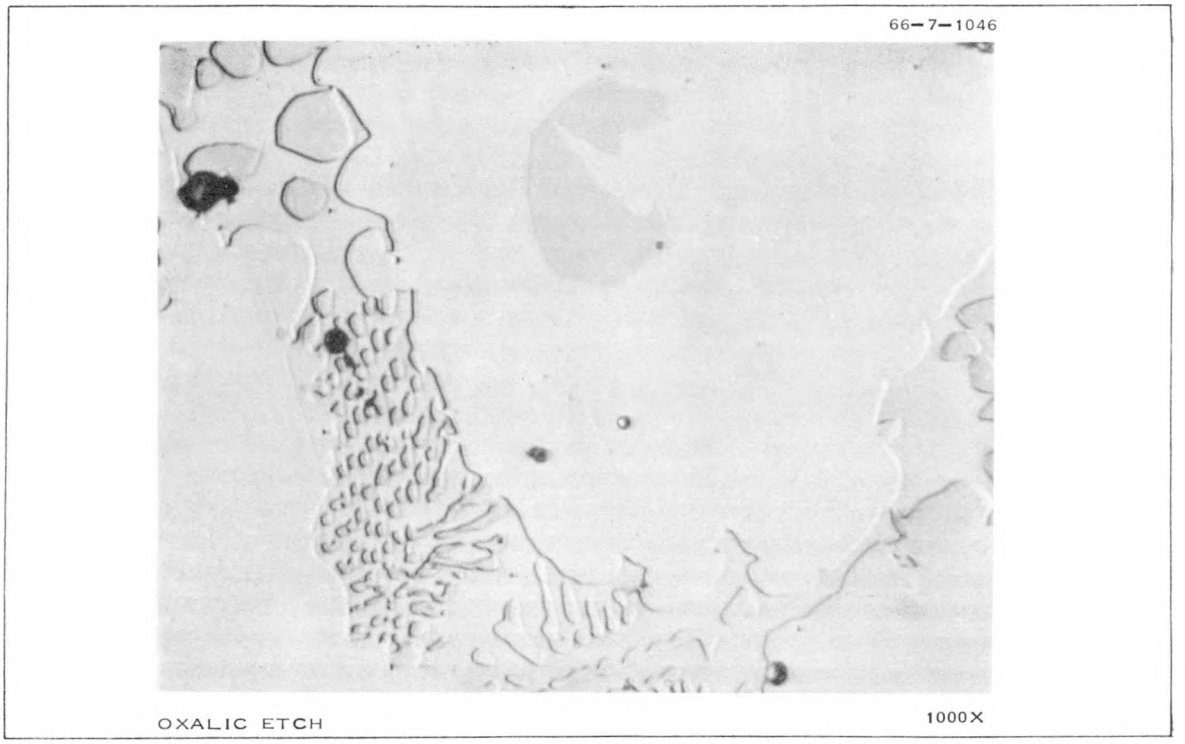

Fig. I-21 Microstructure of Ni-UAl_3 sample, sintered in H_2 at 1200°C.

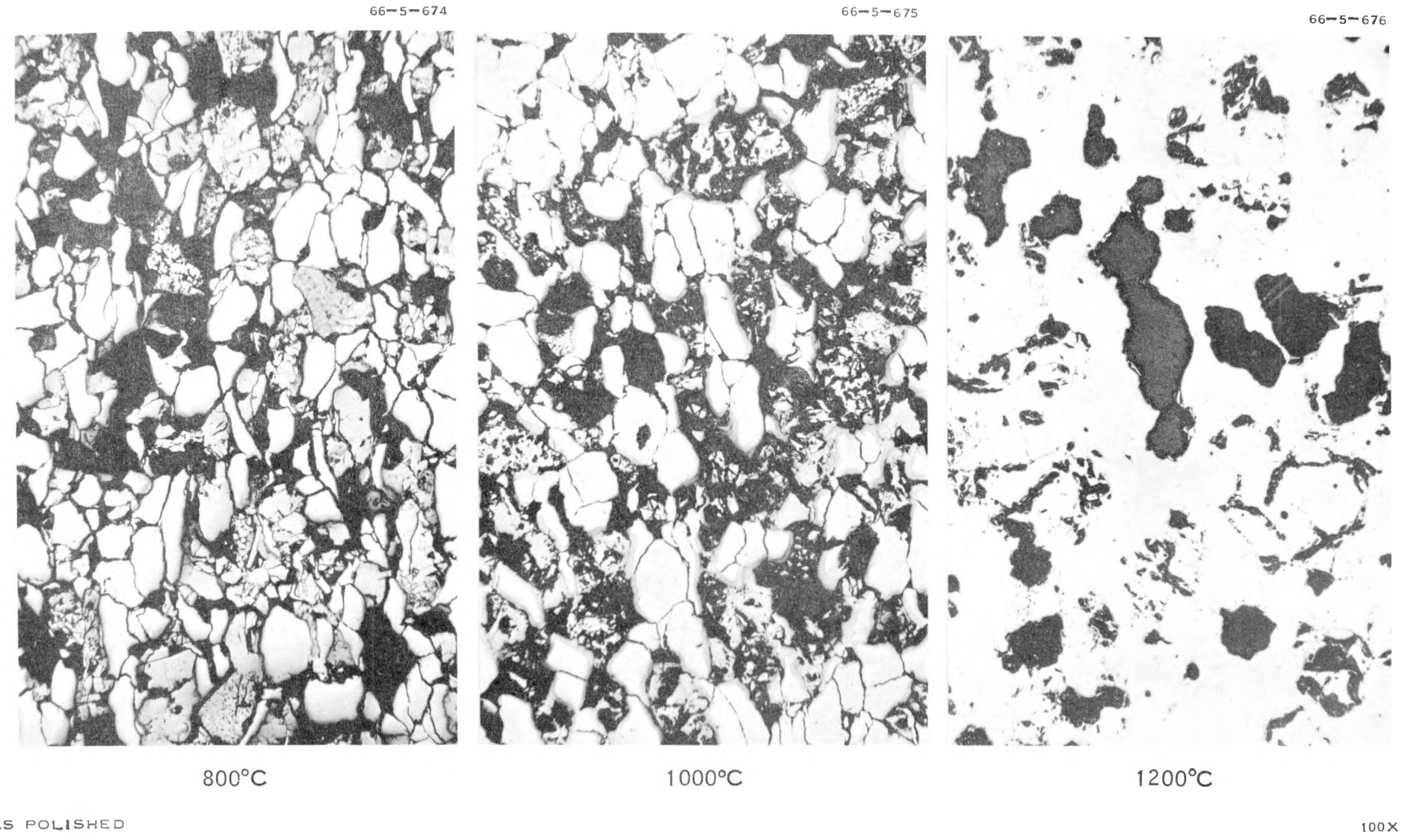

Fig. I-22 Microstructure of Cr-UAl_3 samples, sintered in H_2 at the temperatures indicated.

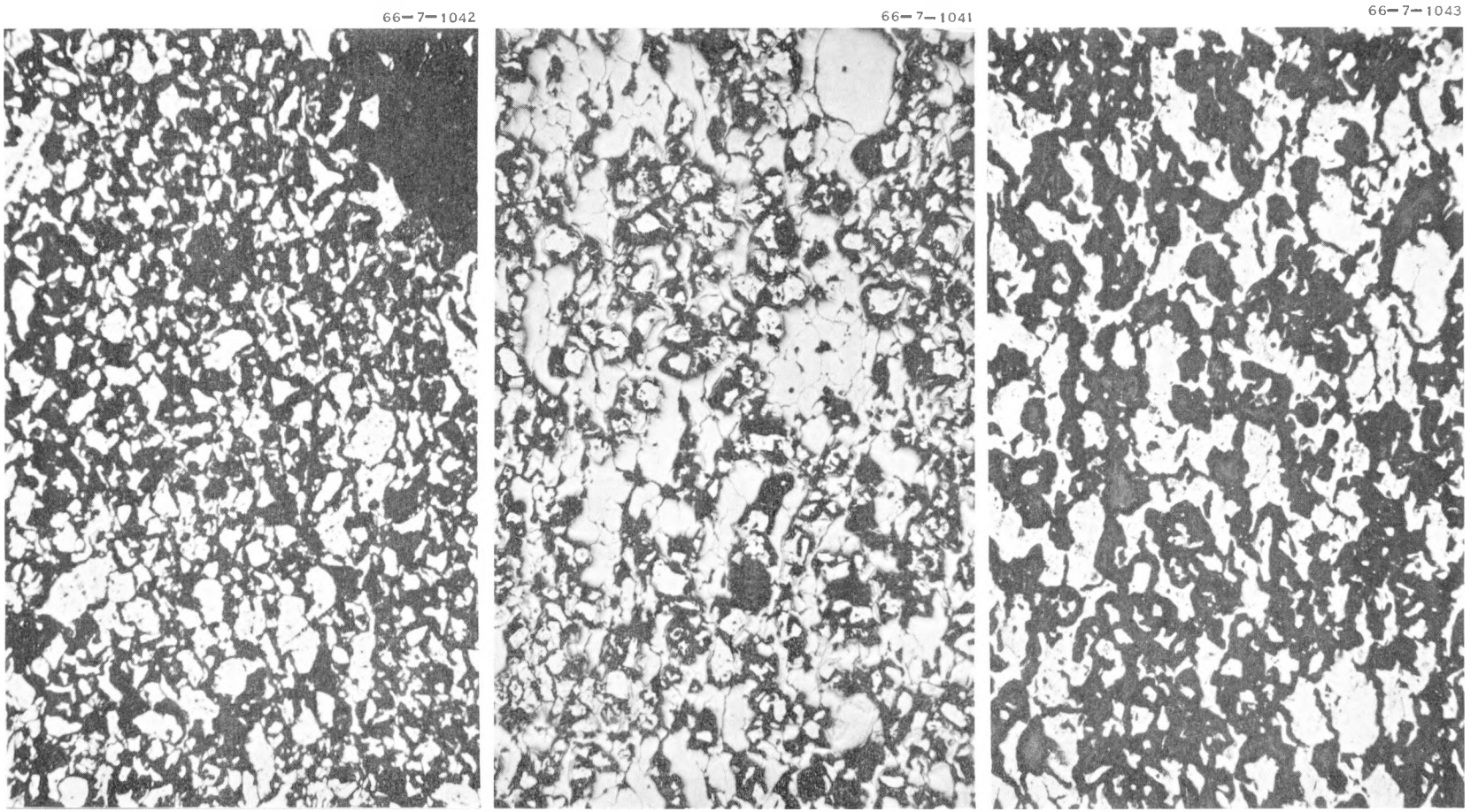

Fig. I-23 Microstructure of Nb-UAl_3 samples, sintered in H_2 at the temperatures indicated.

4. MATERIALS RESEARCH
(J. M. Beeston)

4.1 Microprobe Examination to Determine Compatibility of Fuel Systems Prepared by Powder Metallurgy (W. F. Zelezny, R. A. Moen)

Samples of four possible fuel systems which had been prepared by powder metallurgy techniques were examined by the microprobe to determine diffusion and reactions which could affect the suitability of the various systems for use as fuel materials. Details of the preparation of these powder metallurgy compacts are presented in the previous section of this report.

4.11 UAl_3 - Stainless Steel. An unsintered compact of Type 347 stainless steel containing 35 weight percent UAl_3 which had been hot-rolled at 800°C underwent diffusion and reaction to such a small extent that no reaction zone was shown by microprobe scans or by optical metallography. Electron microscopy at a magnification of 5600X was able to reveal a complex reaction zone about 0.7 microns wide, as illustrated in Figure I-24.

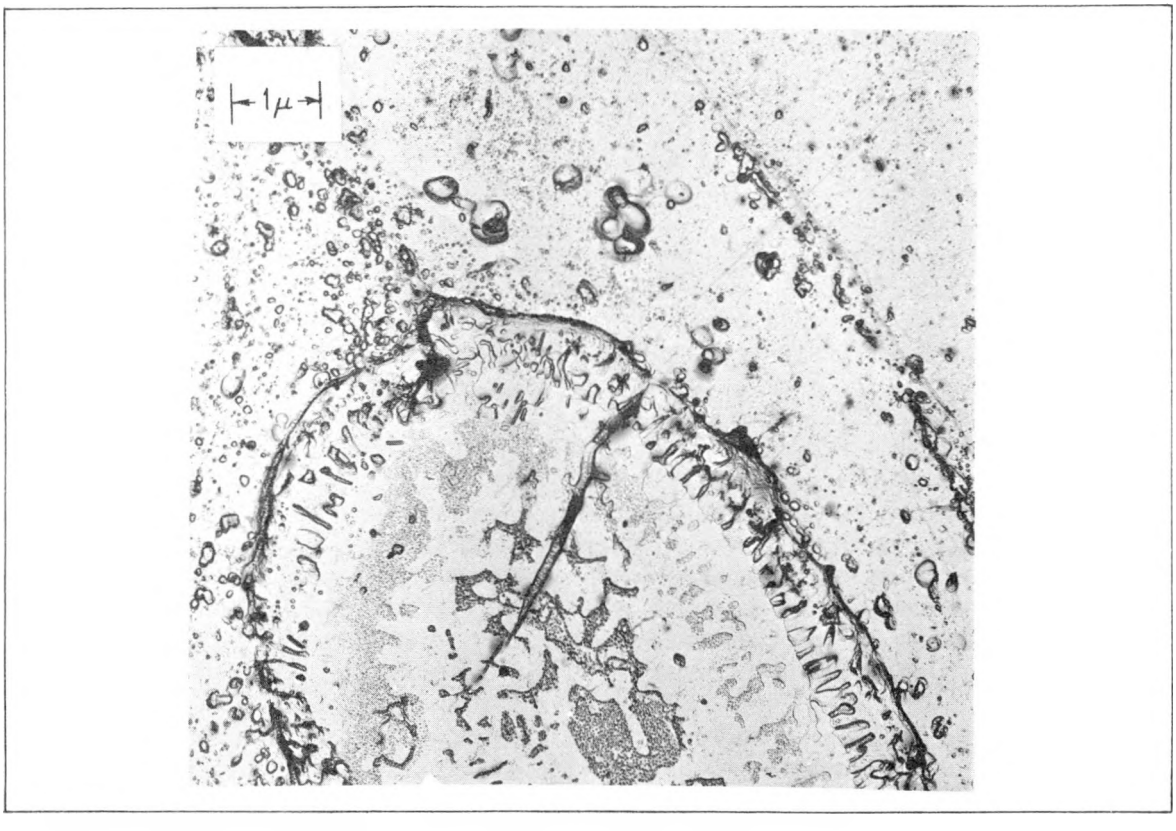

Fig. I-24 Electron micrograph of hot-rolled compact of Type 347 stainless steel - UAl_3 showing complex reaction zone at stainless steel - UAl_3 interface.

Sintering a similar UAl_3-304 stainless steel compact for 8 hours at 1250°C resulted in the complete diffusion of the aluminum into the stainless steel, giving a uniform concentration of aluminum throughout the matrix. The results of this behavior are shown by the microprobe chart recordings reproduced in

Figure I-25. The aluminum, diffusing away from the UAl_3 particles, left behind voids partially filled with uranium. The uranium showed no tendency to diffuse into the stainless steel and remained as discrete particles of uranium.

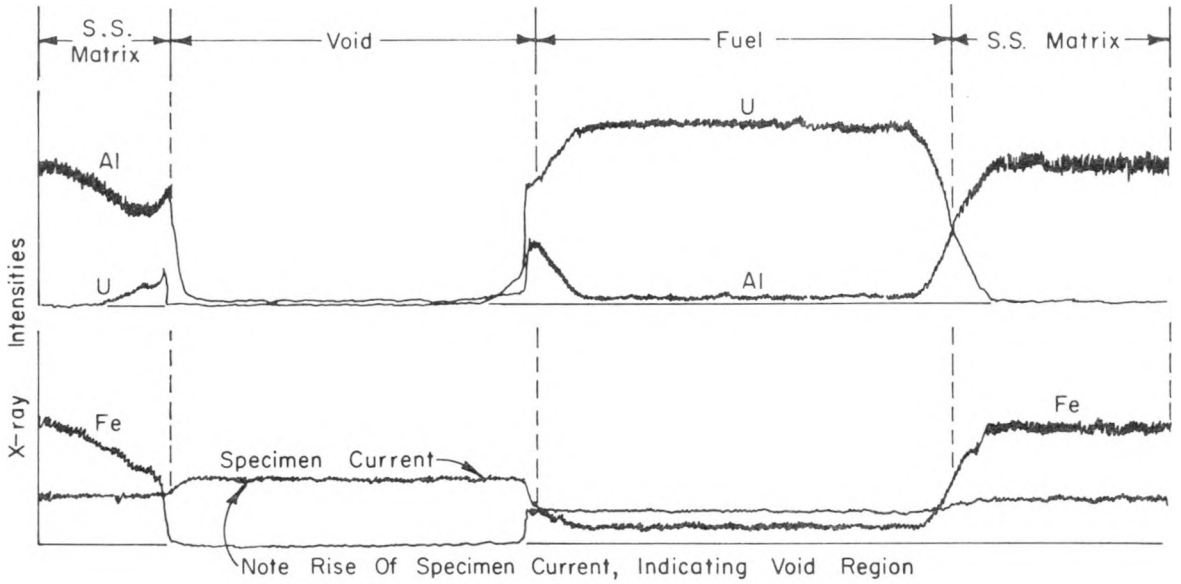

Fig. I-25 Microprobe scan of sintered 304 stainless steel - UAl_3.

4.12 UAl_3-Cr. In this fuel-matrix combination (listed elsewhere in this report as Mount 1226) the aluminum diffused into the chromium for an appreciable distance (15 to 30 microns). This produced voids, with the uranium (still containing some aluminum) left clinging to the void walls, as shown by the photomicrograph and accompanying microprobe chart recordings in Figure I-26. The uranium does not seem to have penetrated the chromium at all. The voids, shown in Figure I-26, were filled with liquid epoxy mounting resin by a vacuum mounting technique and, for this reason, do not exhibit the characteristic appearance of voids in the photomicrograph.

4.13 UAl_3-Ni. A compact of UAl_3 and Ni powders (referred to as Mount 1223), when sintered at 1200°C, underwent extensive diffusion and reaction to produce what seems to be four distinct metallographic regions or phases. The darkest region (see Figure I-27) contains only uranium and aluminum. An over-the-peak count (for maximum sensitivity of detection) did not reveal any nickel at all in this region.

The next darkest phase consists almost entirely of nickel and aluminum and, therefore, must be the aluminide phase with a slightly expanded lattice as reported by X-ray diffraction. Over-the-peak counts for uranium in this phase showed a barely detectable amount present (estimated to be about 0.15 weight percent) which can account for the expanded lattice.

The two lighter appearing phases have not been fully characterized as yet. Each of these two phases contains all three elements, Ni, U, and Al.

4.14 UAl_3-Nb. Of this series of fuel combinations, the UAl_3-Nb system showed no interdiffusion or chemical reaction at 800°C. (The sample examined

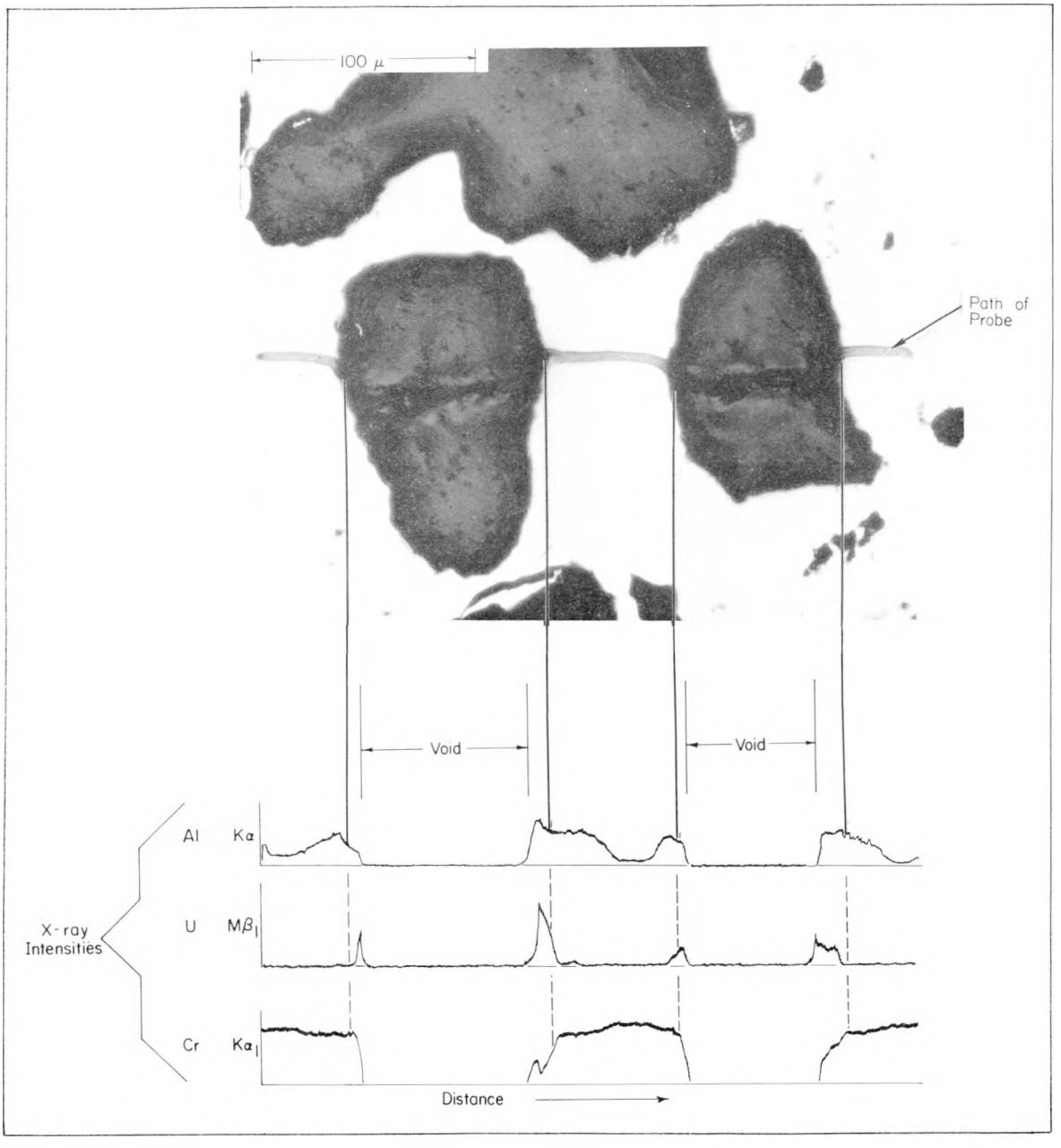

Fig. I-26 Photomicrograph and microprobe scan of UAl_3-Cr powder metallurgy compact sintered for 2 hours at 1200°C in hydrogen (polished, unetched).

is referred to elsewhere in this report as Mount 1257.) Figure I-28 shows that the fuel particles (the lighter particles in appearance) and the Nb matrix (slightly darker gray) have maintained their integrity completely.

The black regions are not voids. In a somewhat inconsistent manner, the black regions sometimes show fuel (U and Al) and sometimes show Nb. Both fuel and matrix material sometimes appear in the same black regions; but within the same black region, the U-Al and the Nb are always separate, never intermixed.

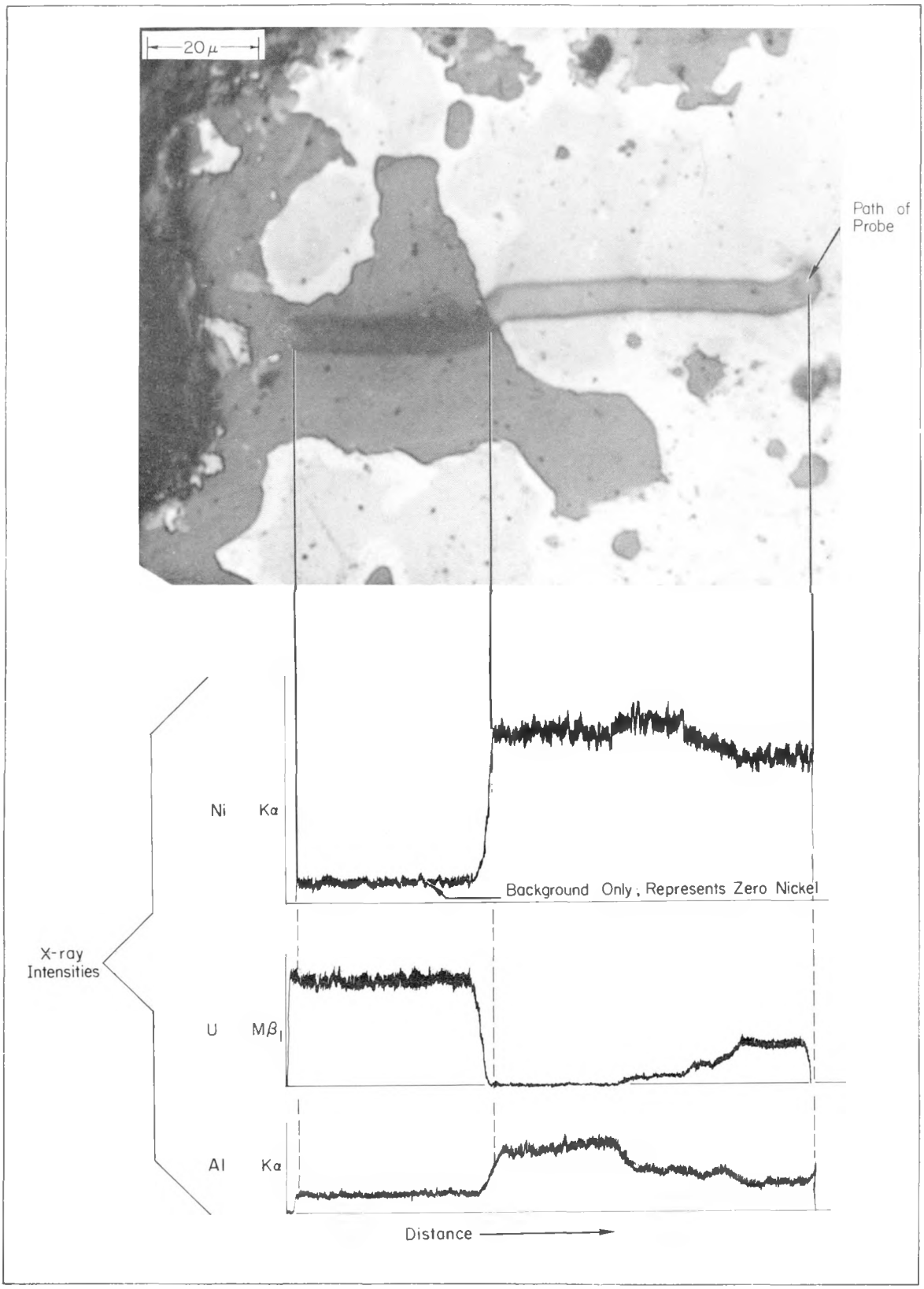

Fig. I-27 Photomicrograph and microprobe scan of UAl_3-Ni powder metallurgy compact sintered for 2 hours at 1200°C in hydrogen (polished, unetched). The jog in the path of the probe scan indicates that the U-Al particle polished in relief.

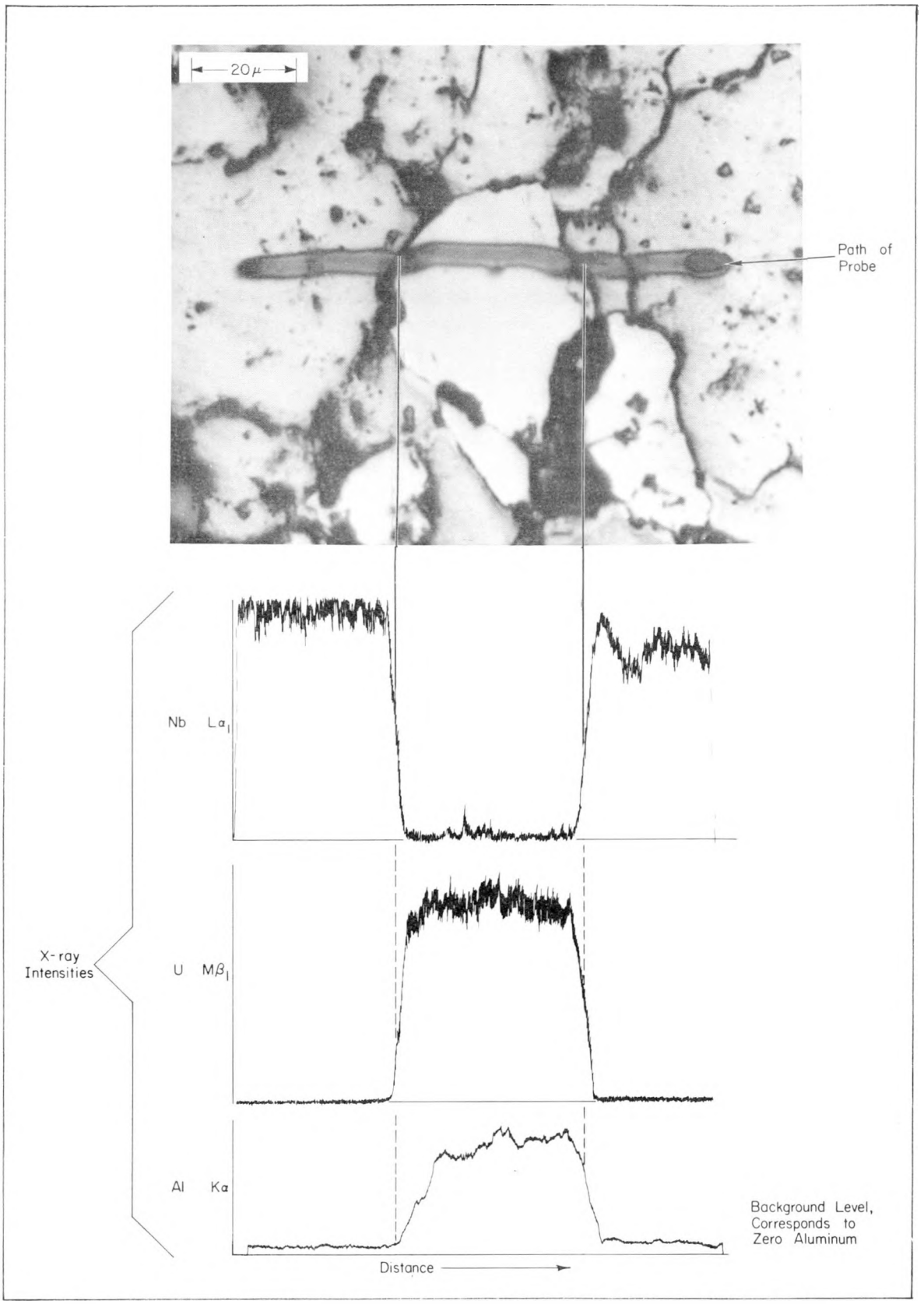

Fig. I-28 Photomicrograph and microprobe scan of UAl_3-Nb powder metallurgy compact sintered for 2 hours at 800°C in helium (polished, unetched).

4.2 Uranium Aluminide Compatibility Studies (R. A. Moen, C. E. May)

Studies are being undertaken to determine swelling and fission gas release in the uranium aluminide fuels, UAl_2, UAl_3, or UAl_4. To evaluate these mechanisms, capsule irradiations will be carried out in which a solid cylinder of the pure aluminide fuel will be unrestrained in a sealed and inert heat transfer medium.

The initial phase of this program involves the selection of a suitable heat transfer medium which will be molten during irradiation, thus permitting the solid cylinder of fuel to grow and release fission gas. The first series of screening tests included samples of powdered UAl_3 (compacted to about 78 percent of theoretical density) and a cast, 21 weight percent, U-Al alloy heated with powdered lead, tin, bismuth, or magnesium at temperatures from 500 to 700°C.

The results of these tests indicated that liquid lead was compatible with the aluminide fuels at temperatures to 600°C for up to 94 hours. The liquid bismuth and tin reacted with the UAl_3, resulting in the formation of many unidentified phases (see Figure I-29). Figure I-30 shows little evidence of attack on the U-Al alloy by either lead, tin, or bismuth. Results from capsules containing magnesium were not obtained due to unexplainable capsule failures.

With the first series of tests showing promising results with liquid lead, a second series of tests was performed utilizing 99.999 percent pure lead and a more sophisticated capsule design. The capsule, as shown in Figure I-31, was constructed of quartz tubing. A stainless steel spring was placed on top of the fuel sample to keep the fuel completely immersed during heating. Upon removal from the furnace, the capsule was inverted from its previous upright position, thus allowing the liquid lead to drain away from the fuel specimen and solidify in the bottom of the capsule.

Materials tested included powder compacts of UAl_3 and UAl_4 and a 70 weight percent U-Al alloy. The UAl_3 was heated with the liquid lead at temperatures from 500 to 900°C while the UAl_4 and U-Al alloy were heated only to 700°C for up to 72 hours. Visual examination of the capsule contents after heating indicated that all materials appeared unattacked to 700°C. Reaction was noted in the UAl_3 heated for 72 hours at 900°C with the lead. A thorough metallographic examination has not been completed.

Pre- and post-test dimensions show a negligible volume change for the UAl_3, about a 1.6 percent volume increase for the U-Al alloy, and a slight decrease in volume for the UAl_4. The increase in size might be explained by swelling due to entrapped gases while the volume decrease, as in the case of the UAl_4, could either be due to sintering or dissolution of the fuel in the lead. The metallographic examination should answer these questions.

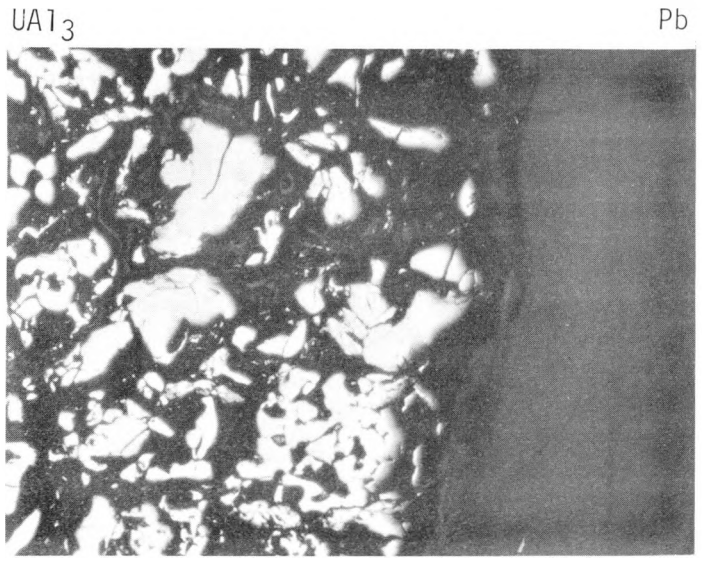

UAl3 heated with liquid lead for 94 hours at 700°C

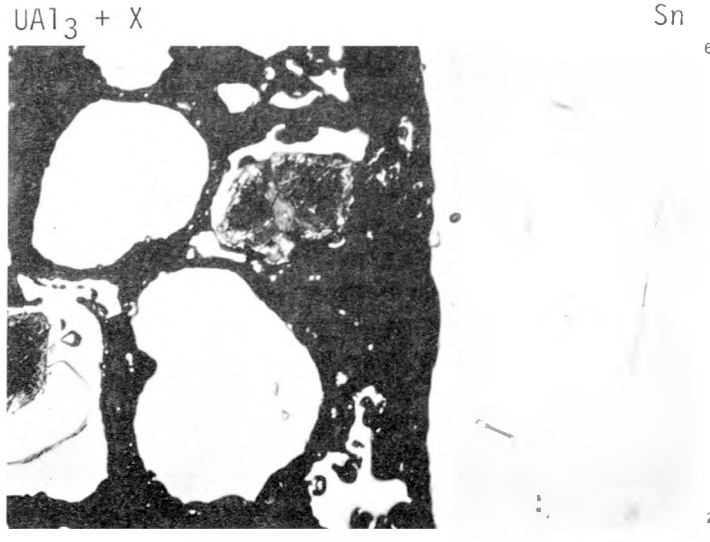

UAl3 heated with liquid tin for 94 hours at 700°C

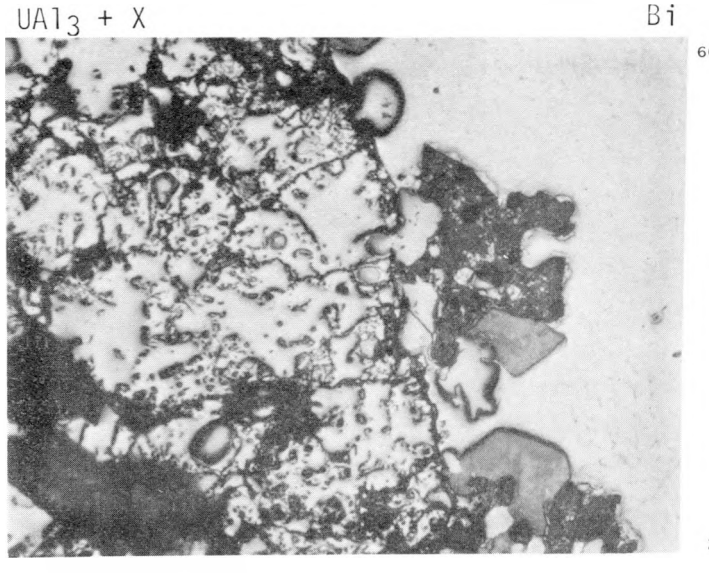

UAl3 heated with liquid bismuth for 94 hours at 700°C

Fig. I-29 Microstructures of powder compacts of UAl_3 after heating at 700°C with various liquid metals (200X).

66-4-645

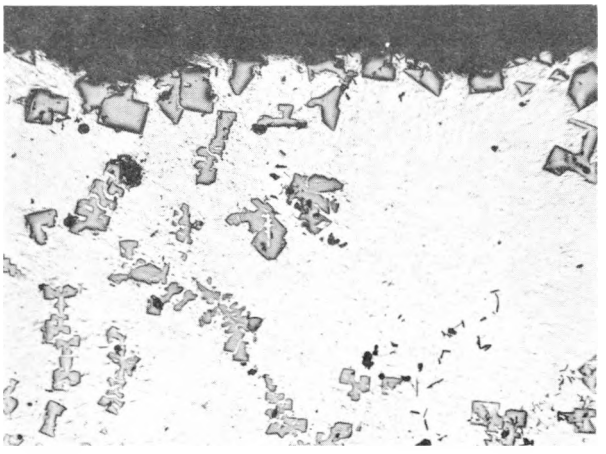

CONTROL SAMPLE
SURFACE OF AS-CAST ALLOY

66-4-651

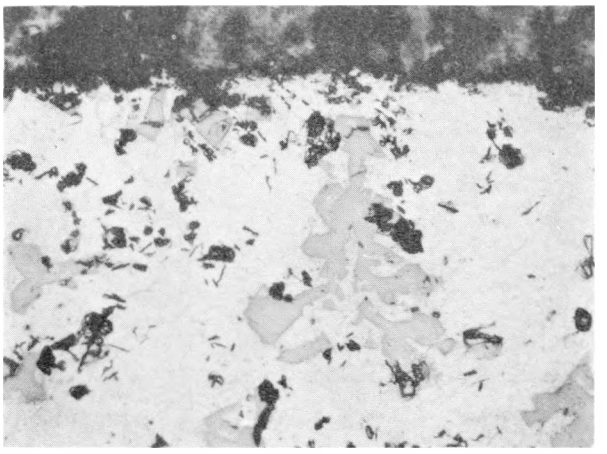

SURFACE OF SAMPLE HEATED WITH
LIQUID LEAD FOR 94 HOURS AT 500°C

66-4-648

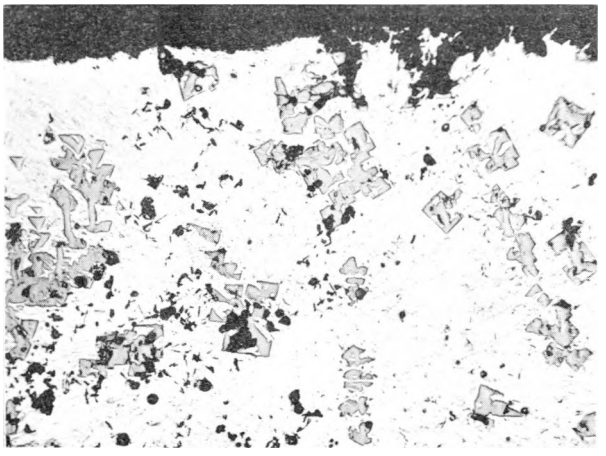

SURFACE OF SAMPLE HEATED WITH
LIQUID TIN FOR 94 HOURS AT 500°C

66-4-647

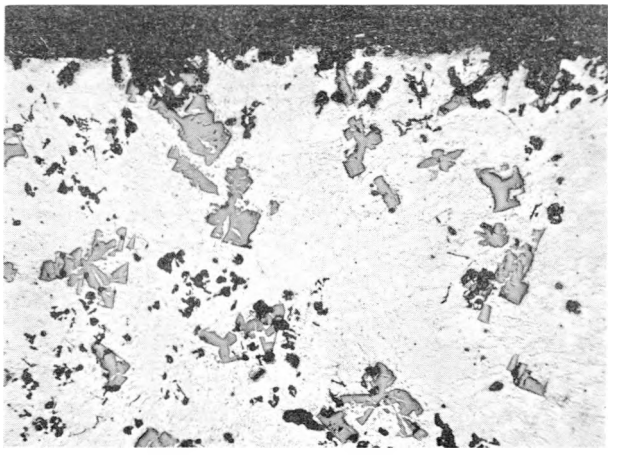

SURFACE OF SAMPLE HEATED WITH
LIQUID BISMUTH FOR 94 HOURS AT 500°C

Fig. I-30 Microstructures of 21 percent U-Al alloy after heating at 500°C with various liquid metals (200X).

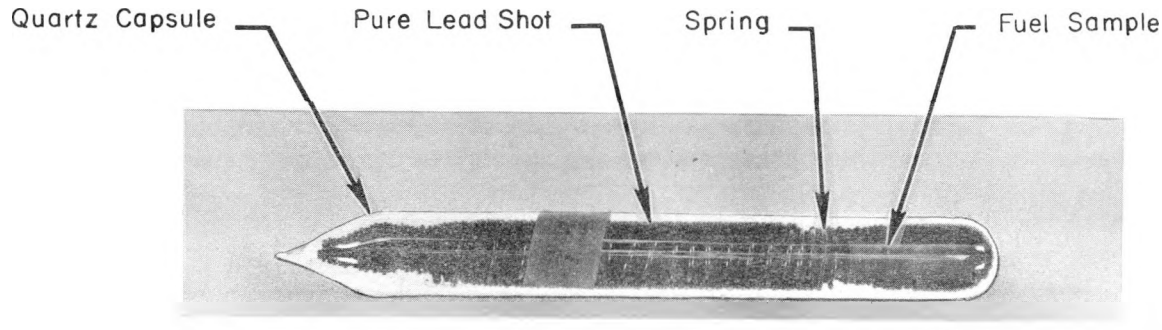

Fig. I-31 Quartz capsule used for the compatibility tests. (Capsule sets upright with the fuel sample at the bottom during heating.)

5. PAPERS PRESENTED

1. R. A. Moen and G. W. Gibson, "Corrosion Behavior of Aluminum Powder Metal Products", presented at the Fifteenth Annual AEC Corrosion Symposium, Oak Ridge, Tennessee.

6. REFERENCES

1. J. L. Durney and J. W. Henscheid, "Power and Flux Measurements in a 39-kg Core in the ATRC", Nuclear Technology Branches Quarterly Report, January 1 - March 31, 1966, IDO-17192 (August 1966) pp 1-4.

2. N. C. Kaufman, "ATRC Fuel Annulus Void Coefficients of Reactivity", Nuclear Technology Branches Quarterly Report, April 1 - June 30, 1965, IDO-17140 (March 1966) pp 4-5.

3. N. C. Kaufman and J. W. Henscheid, "Reactivity Measurements in the ATRC", Nuclear Technology Branches Quarterly Report, October 1 - December 31, 1964, IDO-17081 (July 1965) p 1.

4. N. C. Kaufman, "Effects of Venting ATR Fuel Side Plates", Nuclear Technology Branches Quarterly Report, October 1 - December 31, 1964, IDO-17081 (July 1965) pp 5-9.

5. W. L. Schrader and J. W. Henscheid, "ATR-ATRC Safety Rod Worths", Nuclear Technology Branches Quarterly Report, April 1 - June 30, 1965, IDO-17140 (March 1966) pp 6-7.

6. K. V. Moore, Shutdown Reactivity by the Modified Rod Drop Method, IDO-16948 (March 1964).

7. E. Garelis and J. L. Russell, Jr., "Theory of Pulsed Neutron Source Measurements", Nucl. Sci. Eng., 16 (July 1963) pp 263-270.

8. W. L. Schrader and J. L. Durney, "ATRC Safety Rod Calibrations", Nuclear Technology Branches Quarterly Report, October 1 - December 31, 1964, IDO-17081 (July 1965) pp 10-11.

9. N. C. Kaufman, "Experimental and Calculated Reactivity Distribution for the ATR", Nuclear Technology Branches Quarterly Report, October 1 - December 31, 1964, IDO-17081 (July 1965) p 1.

10. N. C. Kaufman and J. W. Henscheid, "Initial ATRC Experiments", Nuclear Technology Branches Quarterly Report, April 1 - June 30, 1964, IDO-17042 (November 1964) pp 7-10.

11. D. R. deBoisblanc and S. Cohen, Safety Analysis Report Advanced Test Reactor, Volumes 1 and 2, IDO-17021 (April 1965).

12. D. R. deBoisblanc, Nuclear Technology Branches Quarterly Report, January 1 - March 31, 1966, IDO-17192 (August 1966).

13. O. J. Marlowe, Nuclear Reactor Depletion Programs for the Philco-2000 Computer, WAPD-TM-221 (January 1961).

14. M. L. Griebenow and K. R. Dickey, MACABRE, IDO-17096 (November 1965).